The Ignition of Methane and Coal Dust by Air Compression - The Experimental Proof

Wei Lin

Thesis submitted to the Faculty of the Virginia Polytechnic Institute and State University
in partial fulfillment of the requirements for the degree of

Master of Science
in
Mining Engineering

Malcolm J. McPherson, Chair
Michael Karmis
Mario G. Karfakis

May 1, 1997
Blacksburg, Virginia

Keywords: Methane, Dust, Compression, Explosion, Experiments

The Ignition of Methane and Coal Dust by Air Compression
-The Experimental Proof

Wei Lin

(ABSTRACT)

When a large area of open gob collapses suddenly, a windblast is produced that can cause considerable damage throughout the infrastructure of a mine. In a few cases, the windblast has been accompanied by ignitions of methane and/or coal dust. Analytical and numerical analyses investigated the transient behavior of the air through the small time period during which the roof is falling. This is sufficiently short to allow adiabatic compression of the air, i.e. negligible heat transfer to rock surfaces. Controlled escape of the air via interconnecting entries limits the build-up of air pressure. However, this same phenomenum causes the potential energy of the falling strata to be concentrated into a diminishing mass of air. Computer simulations predicted that the temperature of the air would increase rapidly as the roof descends, reaching values that are capable of igniting either methane or coal dust.

This thesis concentrates on a series of laboratory tests involving the compression of mixtures of air, methane and coal dust under a falling weight and while allowing controlled escape of the mixture. The transient responses on pressure and temperature sensors were recorded. In addition to an analysis of those records, the thesis highlights those conditions in which ignitions occurred.

Acknowledgments

I wish to express my sincere appreciation to Dr. McPherson, my academic advisor and committee chairman, for his guidance and help throughout this study.

I wish to thank, also, the members of my committee, Dr. Karfakis and Dr. Karmis.

I would like to recognize the effort of Mr. Wayne of the Department of Mining and Minerals Engineering, who assisted with the construction of the test rig and with the set-up and conduct of the tests. I also thank Dr. Loomis, a former Ph.D student of this department, who helped me to complete the laboratory tests.

More than two years in the Department of Mining and Minerals Engineering at Virginia Tech have been a wonderful and unforgettable experience. I wish to thank all the people in the department who helped me with my study and life.

Table of Contents

List of Figures

List of Tables

List of Plates

Chapter 1. Introduction

1.1 THE PROBLEM STATEMENT

Throughout the history of mining industry, there have been a number of recorded cases of mine explosions being triggered by large roof collapses in the various underground openings. The occurrence of a collapse is mainly caused by a pillar's failure or behind a longwall face. When a large area of underground mined-out workings collapses suddenly, the air beneath the roof beds is compressed very rapidly. The pressurized air is dissipated subsequently at a rate controlled by the resistance of the leakage paths. The rapid compression of air will give rise to a pressure shock wave that will be transmitted through the remaining workings as an air blast (McPherson, 1980).

The air blast produced by large roof falls can cause serious damage to equipment and injury to personnel throughout the infrastructure of a mine. In fact, there have been reports that the air blast caused by large roof collapses has been accompanied by ignitions of coal dust and/or methane. In an underground mine, especially in a coal mine, the basic conditions which are needed to initiate a coal dust explosion are the formation of a coal dust cloud and its ignition. Normally, under conditions prevailing in mines, coal dust accumulates on the surfaces in the workings while the quantities of this dust in the air are entirely insufficient to develop an explosion; in the other words they are much lower than their lowest explosive limits.

Two factors must act synchronously to initiate a coal dust explosion: a factor which will cause the raising of a dangerous cloud of coal dust and the appearance, at the same time, of a thermic factor capable of igniting this cloud (Waclaw, 1975). The air blast created by a large roof fall raises easily a dangerous cloud of coal dust. There are, at least, three thermic sources of ignition. One of these is that incendiary streaks which are able to ignite a dust-methane-air mixture can be produced by sliding friction between blocks of falling sandstone or pyrite, or between rock and steel, especially when the strata contains a quartz exceeding some 20 percent (Powell and Billinge, 1975). Secondly, the violent air blast accompanied by an explosive mixture of dust, methane and air into active workings may destroy electrical or other equipment to the extent that a thermic source is was generated. Thirdly, lightning strikes on surface have also been suspected of traveling into areas of the mine where dust-methane-air mixtures had accumulated, igniting the gases (Elio and David, 1995).

A recent analysis (McPherson, 1995a) has indicated that there is the existence of another thermic source. The adiabatic compression of the air under a fall of large areal extent can produce air temperatures that may be well above those necessary to initiate a gas or coal dust explosion. In underground coal mines, the presence of methane increases greatly the possibility of ignition. The coal dust and methane are synergistic.

1.2. CASE STUDY

1.2.1. Coalbrook Colliery, South Africa

The disaster which occurred at Coalbrook Colliery in South Africa on 21th January, 1960 resulted in the loss of 437 lives and arose from the collapse, over an area of at least 750 acres, of the whole mass of the strata between some of the pillar workings in the No. 2 Seam and the surface on the east side of the colliery. This seam, the only one worked in the part of the mine affected by the disaster, is about 25 ft thick and lies at an average depth of nearly 470 ft from the surface. The disaster was rare in at least two respects. One is that the loss of life was the highest ever recorded for this kind of occurrence. Secondly, during a short period of five minutes, the complete subsidence of such an extensive mass of strata above mine workings was unprecedented (Byran et al, 1964).

1.2.2. Wa Jing Wan Colliery, China

Wa Jing Wan Cooliery is one of the operating mines of the Datong Mineral Bureau in China. In the 832 mining area of 402 panel at qing Yangwan shaft of this mine, the room-and-pillar mining method is used to extract a Jurassic coal seam to a height of m to 4.3 m. The compressive strength of the immediate hard roof is over 100 MPa. The average thickness of the strata varied from 5 m to 10 m, occasionally, up to 40 m. In the early 1960s, severe air blasts produced by the caving of large area of roof occurred. In July, 1960 an area of 22,310 m^2 roof caving caused one fatality and twelve injuries. The damage spread even to the surface, producing surface cracks ranging from 60 m to 70 m in length, and surface subsidence of 0.3 m to 0.7 m. When the mined-out area reached to approximately 163,000 m^2 on October 22, 1961, the roof caved entirely. The devastating windblast resulted in 14 deaths, 19 injuries, and severe damage to the mine facilities and ventilation system (Song and Xu, 1992).

1.2.3. Moura No.4 Coal Mine, Australia

At Moura No.4 coal mine in Australia, an area of the mined-out workings estimated at some 10,000 m^2, within a larger total gob, collapsed on July 16th, 1986. The seam was extracted to a total height of 5 m. The overlying strata was composed of some 60 m thickness of laminated sandstones up to the next superadjacent coal seam. The rectangular gob area was bounded by solid coal on three sides with five entries connected to the operating zone on the fourth side. The windblast that swept through this section was either accompanied or followed immediately by a coal dust explosion. All twelve miners in this section were killed (McPherson, 1995b).

The above are only few cases among many in which the devastating windblasts were accompanied when a large roof collapsed suddenly. In some cases, coal dust explosions were accompanied or followed. The research described in this thesis employed laboratory simulation instruments to examine whether an ignition can occur while the air is adiabatically compressed.

Chapter 2. Background Theory

Mine explosions have been a leading killer in underground coal mine operations. There are many reasons related to mine explosions. Among them are the friction, electrical equipment, explosives and lightning strikes ignitions. People have known for a long time that the air blast produced by an extensive area collapses in underground mining can cause extensive damage to personnel and equipment, perhaps even reaching to surface plant. Early in 1980, Dr. McPherson conducted some fundamental work on the air pressure developed in collapsing mine working. He stated that the maximum air pressure is reached very quickly after pillar failure has occurred and there will be a considerable increase in temperature during the compression.

In his more recent work (McPherson, 1995), he first proposed the ignition possibility because of the increase in temperature of air due to adiabatic compression under the falling roof. According to this theory, the temperature of the air increases rapidly and continuously as the roof descends, reaching values that are capable of igniting either methane or coal dust. The theory is based on following assumptions. First, that during roof falls, because the heat transfer to the surrounding rock mass occurs very slowly compared with the rapid air compression process, the air compression process is adiabatic. Second, that in order to consider the more real situation that the floor and falling roof were not perfectly smooth, and that roof began to break up during the fall, there is a mean effective gap between the floor and the broken roof material. Third, that the treatment of the escape of air from the collapsing zone has been based on steady-flow relationships and, hence, has not taken into account the inertial effects of accelerating the air nor the formation of shock waves within that escaping air.

The air pressures produced under a falling material depend, not only upon its weight and dimensions, but also on the rate at which the air can escape from the area. There are two situations which we need to deal with. One is the idealized situation, the bounded system (no leakage paths out of the zone). The other is the more real situation, the leakage system (leakage paths connected with the zone). The derivative process of all equations in this chapter is from the work of McPherson. Before dealing with air leakage situation, and in order to facilitate the introduction of a quantified analysis, we shall first examine the idealized situation of a closed system with no leakage.

2.1. THE BOUNDED SYSTEM (NO LEAKAGE)

The bounded system is an idealized state. Figure 2.1 shows that air is compressed beneath a falling mass in a bounded system (no leakage). In this situation, the air is contained completely in the space under the falling materials. If there are no frictional effects, the net force exerted on the falling mass arises from the combined effects of its

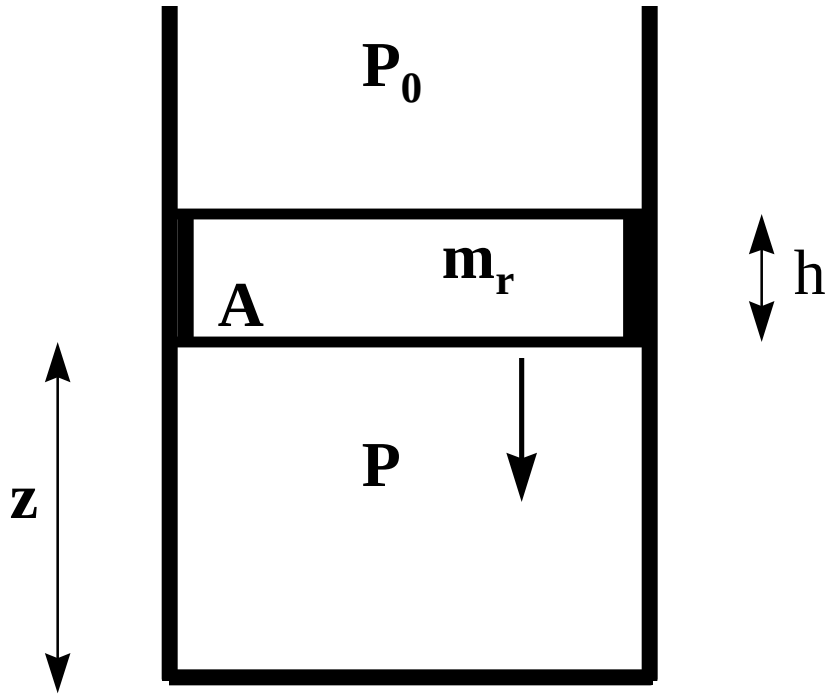

Figure 2.1. Air is compressed beneath a falling mass in a bounded system (no leakage) (after McPherson, 1995a).

weight and the pressure different across it:

$$F = m_r\, g + (P_0 - P)\, A \qquad N \qquad (1)$$

where,
F = the net force exerted on the falling mass (N),
m_r = mass of the falling slab (kg),
g = gravitational acceleration (taken as 9.81 m/s^2 in this analysis),
P_0 = air pressure over the falling slab (Pa),
P = air pressure under the falling slab (Pa),
A = plan area of the falling slab (m^2).

At any given time, t , the velocity of the falling slab is u (m/s) and its acceleration is $a = \frac{du}{dt}$ (m/s^2). Then, as follows :

$$F = m_r \, x \, a$$
$$= m_r\, g + (P_0 - P)\, A = m_r \frac{du}{dt} \qquad N \qquad (2)$$

where,

u = velocity of the falling block (m/s).
giving :

$$du = \left[g - \left(P - P_0 \right) \frac{A}{m_r} \right] dt \qquad m/s \qquad (3)$$

Now, if the plan area of the falling slab is A (m^2) and its thickness is h (m), then the mass of the slab is as follows:

$$m_r = Volume\ of\ rock\ x\ rock\ density$$
$$= A\ h\ \rho_r \qquad kg$$

or

$$\frac{A}{m_r} = \frac{1}{h\rho_r} \qquad (4)$$

where,
ρ_r = rock density (kg/m^3).

Let us turn now to the compression process undergone by the air beneath the falling slab. The process is essentially adiabatic as there is very little time for heat transfer to occur between rock surfaces and the air during the compression. It will follow the law:

$$PV^k = constant = C' \qquad (5)$$

where,
V = volume of gas (m^3),
k = the adiabatic index (1.4 for dry air),
C' = constant.
However,

$$V = A\ x\ z \qquad m^3 \qquad (6)$$

where,
z = distance between the floor and the falling roof (m).
giving:

$$P\ (A\ x\ z)^k = C' \qquad (7)$$

$$P\ z^k = C \qquad (8)$$

or

$$P = \frac{C}{z^k} \qquad Pa \qquad (9)$$

The constant, *C*, can be determined from the initial conditions:

$$P = P_0 \qquad (10)$$

and

$$z = z_0 \qquad (11)$$

i.e.

$$C = P_0 z_0^k \qquad (12)$$

Now, substituting for $\frac{A}{m_r} = \frac{1}{hr_r}$ (eq. 4) and $P = \frac{C}{z^k}$ (eq. 9) into equation (3) gives:

$$\frac{du}{dt} = \left[g - \left(\frac{C}{z^k} - P_0 \right) \frac{1}{hr_r} \right] \qquad m/s^2 \qquad (13)$$

Equation 13 describes the motion for an undamped and totally bounded system. In such a situation, the falling slab would compress the underlying air and bounce back to its initial position, repeating this process indefinitely. In reality, shear resistance at the sides of the falling slab, couple with turbulence generated within the compressed air will cause the system to be damped. It will then oscillate with decreasing amplitude until it comes to rest. The damping forces depend upon the velocity, *u*, the contact area between the sides of the falling block and the intact rock mass, and the initial air volume to be compressed below the falling block. For the purposes of this analysis, the damping effect has been taken into account by means of a damping factor, *DF*. Equation (13) can be modified as:

$$\frac{du}{dt} = \left[g - \left(\frac{C}{z^k} - P_o \right) \frac{1}{hr_r} - (\pm) DF * u \right] \qquad m/s^2 \qquad (14)$$

where,
$\pm$ means that damping forces always oppose the motion of the falling block.
The corresponding air temperatures are given by the adiabatic process equation:

$$T = T_0 \left(\frac{P}{P_0} \right)^{\frac{k-1}{k}} \qquad K \qquad (15)$$

where,
T = absolute temperature under the falling block (K),
T_0 = initial temperature when roof fall commences (K).

Equation (9) to (15) can be tracked numerically to show the variations of roof height, z, pressure, P, velocity, u, and temperature, T with respect to time, t. Appendix gives the original computer program written by Dr. McPherson using BASIC language. Figure 2.2 shows the behavior of the system where initial height of roof (z_o) = 5m, initial air pressure (P_o) = 100 kPa, initial temperature = 20 ^{o}C (T_o = 293 K), thickness of falling slab (h)= 4m, rock density (ρ_r) = 2200 kg/m^3 and damping factor (DF) = 3. If reducing the damping factor, the appearance of these curves looks different having more bouncing times with decreasing amplitude.

The absence of air leakage gives these curves a very distinctive appearance that would be realistic for a pneumatic shock absorber or a lubricated but well-fitting piston falling under its own weight into an open topped cylinder. The falling block comes to rest and is supported by the air which (at equilibrium) is compressed to an absolute pressure of 186 kPa or gauge pressure of 86 kPa. The latter is simply the pressure exerted by the weight of the falling slab ($\rho_r gh$). The temperature follows from equation (15) and, hence, gives a similar appearance to the pressure curve.

2.2. THE LEAKAGE SYSTEM

In an actual roof fall situation, the air being compressed will not be confined to the space immediately under the descending roof but will be dissipated through the leakage paths connected to the collapsing area, and then through the mine infrastructure to the surface. The rate of air leakage is affected by: (a) the rapidly escalating resistance to air movement within the collapse zone as the roof descends, (b) the resistance offered by shock and frictional losses as air dissipates into and through the adjacent leakage paths, and (c) the resistance of the remaining flow paths to the surface of the mine. The movement of the air may be conceptualized as shown on Figure 2.3.

Let us consider these situations. Assuming that the falling roof is rectangular with plan dimension of X by W, and that the underlying air is dissipated in the X direction. The rational turbulent resistance of the flowpath under the falling roof in the gob can be estimated as (McPherson, 1995a):

$$R_{fall} = \frac{fX}{2W^2Z^3} \qquad m^{-4} \qquad (16)$$

where,
R_{fall} = rational turbulent resistance of the flowpath under the falling roof (m^{-4}),
f = Darcy coefficient of friction, dimensionless,
X = length of the falling block (m),
W = width of the falling block (m).

From the cubed term, it is clear that the resistance to air clearance from below the fall will increase rapidly as the roof approaches the floor. However, the analogy with steady state airflow cannot really be justified in such a dynamic situation.

The resistance of the adjoining (connected) entries and associated shock losses, R_{conn}, and of the remaining (infrastructure) flowpaths to the surface, R_{infra}, can be assessed from the relevant geometries and ventilation network of the mine.

$$R_{shock} = \frac{shock\ loss\ factor}{2A_a^2} \qquad m^{-4} \qquad (17)$$

where,
R_{shock} = rational turbulent resistance of the flowpath under the falling roof (m^{-4}),
A_a = cross sectional area of the leakage airpath (m^2),

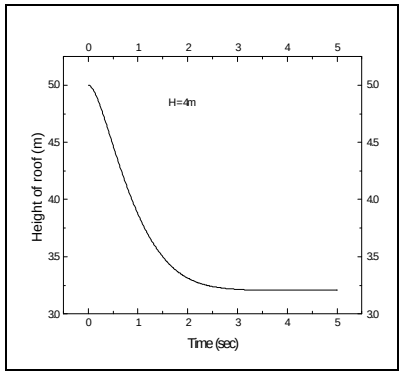

(a)

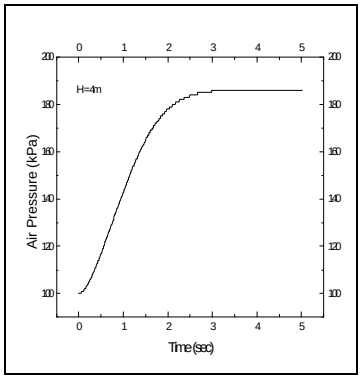

(b)

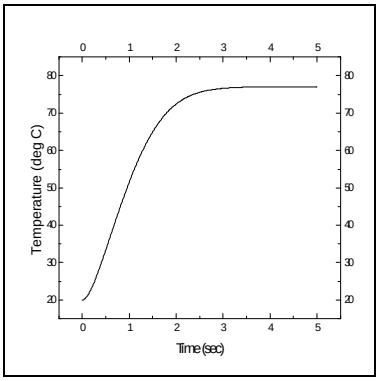

(c)

Figure 2.2. Example of the variation in roof height (a), air pressure (b) and temperature (c) under a 4m thick falling slab with a damping factor 3 and no leakage.

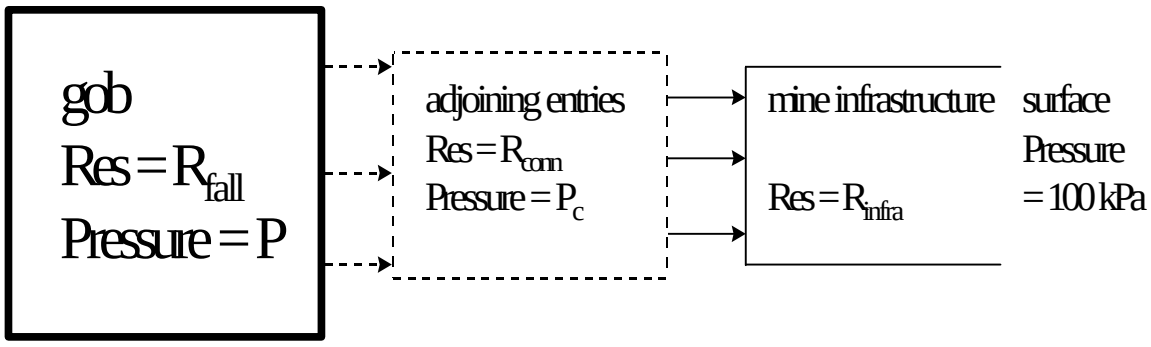

Figure 2.3. Flowpaths of air escaping from collapsing gob
(after Wei. L and McPherson, 1996)

shock loss factor = the order of 1 velocity head.

$$R_{length} = \frac{fL_aS}{2A_a^3} \qquad m^{-4} \qquad (18)$$

where,
R_{length} = rational turbulent resistance at entry from the collapse zone to an airway (m^{-4}),
L_a = length of the leakage airpath (m),
S = perimeter of the leakage airpath (m).
The resistance of a single connecting airway, R_i, becomes:

$$R_i = R_{shock} + R_{length} \qquad m^{-4} \qquad (19)$$

In the case of multiple airways connected into the collapse zone, their combined resistance can be assessed by assuming that they act in parallel:

$$R_{conn} = \left(\sum \frac{1}{\sqrt{R_i}} \right)^{-2} \qquad m^{-4} \qquad (20)$$

where,
R_{conn} = effective combined resistance of the adjoining entries and associated shock losses.
R_{infra} can also be obtained from the relevant geometries and ventilation network of the mine.

Next step is to determine the rate of air loss from the falling area. Suppose that the mass of the air under the falling roof is m_a, and that due to air loss this reduces by dm_a in a very short time interval, dt. The rate of mass flow during this time may be stated as:

$$M = \frac{dm_a}{dt} \qquad kg/s \qquad (21)$$

However, from the square law for compressible flow, the rate at which air mass is displaced from under the falling roof into the connected entries, $\frac{dm_a}{dt}$, is governed by the difference in air

pressure between the collapsing area, P, and the immediately adjoining airways, P_c, and is also dependent upon the resistance of the associated leakage paths, R_{conn} (McPherson, 1993):

$$P - P_c = \frac{R_{conn}}{\rho_a} M^2 \qquad Pa \qquad (22)$$

or

$$M = \left(\frac{(P - P_c)\rho_a}{R_{conn}} \right)^{0.5} = \frac{dm_a}{dt} \qquad kg/s \qquad (23)$$

where,
P_c = air pressure of the immediately adjoining airways (Pa),
ρ_a = prevailing air density (kg/m^3),
m_a = air mass remaining under the falling roof, $m_a = \rho_a V$, (kg).

Hence, the mass of air lost from the collapsing area in time dt is:

$$dm_a = \left(\frac{(P - P_c)\rho_a}{R_{conn}} \right)^{0.5} dt \qquad kg \qquad (24)$$

From the general gas law, the reduction in air pressure caused by this loss of air is:

$$dP = dm_a \frac{RT}{V} \qquad Pa \qquad (25)$$

where,
dP = the reduction in pressure due to air loss (Pa),
R = gas constant (287.04 J/kg ^{o}C for air),
V = volume of space beneath the falling roof, $V = z \times X \times W$ (m^3).

During the time stepping procedure of the numerical simulation, stability was achieved at time increments of 0.0001 seconds. At each increment, the increase in air pressure in the gob area due to the falling roof was first calculated, followed immediately by a decrease of dP due to the leakage of mass dm_a.

A similar procedure was employed to track the corresponding movement of air from those immediate entries through the rest of the mine to surface. In this case, the pressure difference was P_c - P_o , where P_o was maintained at 100 kPa. (Figure 2.3).

In this research, we assume that both floor and falling roof were not perfectly smooth, and that the roof began to break up during the fall. Hence, there was a gap between the floor and the broken roof material.

A example of the results of computer simulation is given in Figure 2.4. In this example, the thickness of falling strata = 25m, initial height of workings = 4m, plan area = 100m x 100m, rock density = 2200 kg/m^3 and final effective height of roof in gob = 15cm.From Figure 2.4, the roof descends to near the floor in about 1.5 seconds, then exhibits a single oscillation before settling into its equilibrium position when a mean effective gap of 15 cm remains in the voidages between the floor and broken roof material. The effect of that oscillation is seen on the gob air pressure trace. That reaches an initial peak of some 1000 kPa (absolute) with a corresponding air temperature of approximately 500 ^{o}C. The second peak of pressure is interrupted by the roof material reaching its final position, after which continued dissipation of the air from the gob results in the air pressure falling to normal atmospheric conditions. However, the air temperature continues to ascend during the final stages of the collapse and, because of heat transfer with the rock, becomes indeterminate after movement of the roof has ceased. The trace of air pressure in the airways immediately connected to the gob area shows that personnel and equipment would be subjected to a pressure pulse reaching 360 kPa absolute (i.e. 2.6 atmosphere gauge pressure).

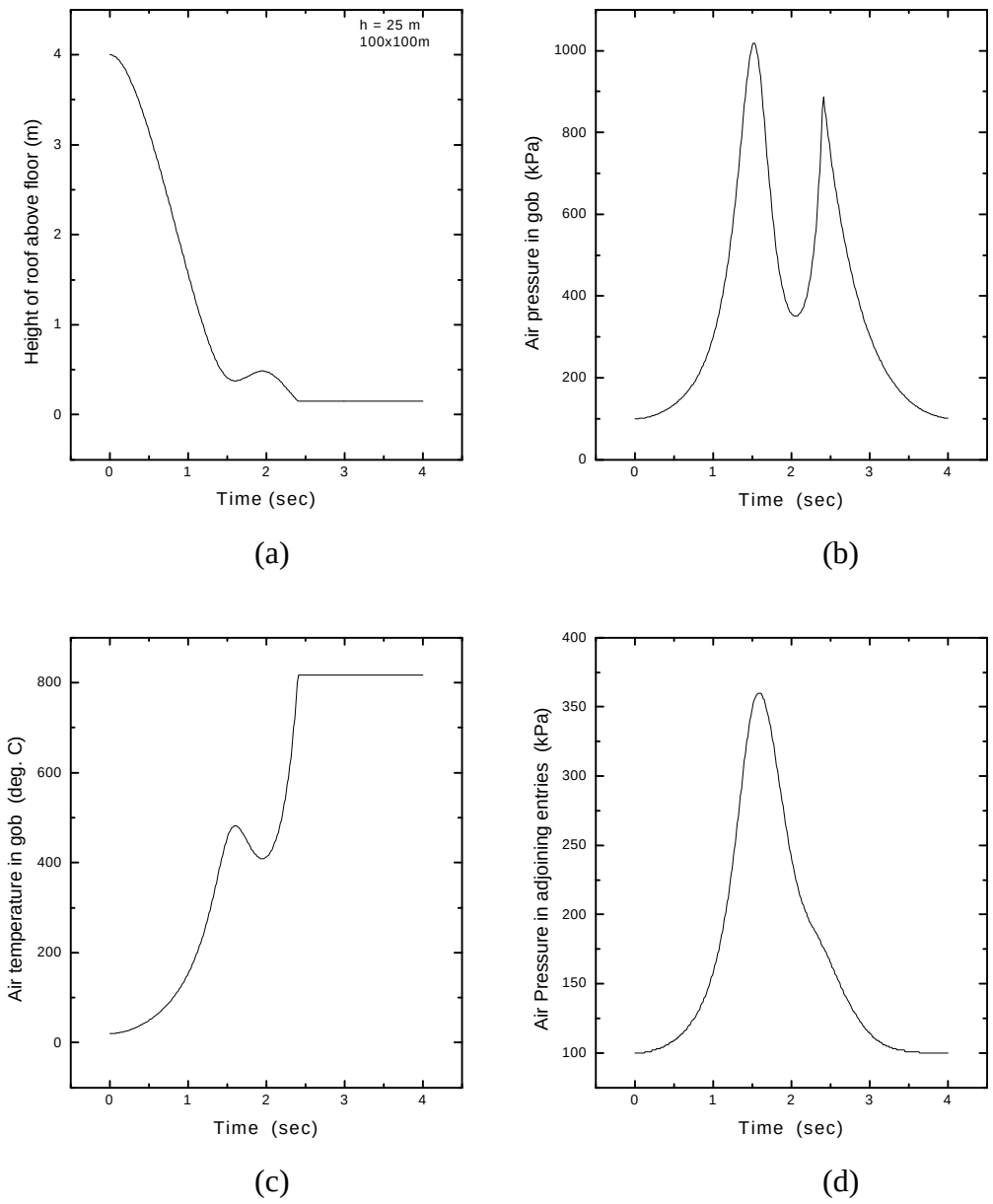

Figure 2.4. Example of transient variations in height (a), air pressure in gob (b), air temperature in gob (c) and air pressure in adjoining entries (d).

Chapter 3. The Setup of Laboratory Tests

3.1. TEST PURPOSE

Liberation of methane in coal mines is continually increasing in extent as result of higher methane content in coal beds and deposits. This is caused by deepening of the mine and the intensification of production, leading to changes in gas content of the coal mines. There exists a large amount of methane in the working and worked-out areas (Lidin, 1964). In addition, the existence of coal dust is unavoidable as long as the coal mines are in production. The existence of methane and/or coal dust increases largely the possibility of a gas and/or dust explosion when the ignition sources occur. There are many kinds of ignition sources, such as electricity, friction and lightning etc. Currently, it is suspected that a large roof fall may also be a possible ignition source (McPherson, 1995a). This fall will compress air adiabatically and produce air temperatures that may be well above those necessary to ignite a gas and/or coal dust explosion.

In order to verify the possibility of explosion of an air, coal dust and/or methane mixture under a large falling roof and get a better understanding about the mechanism of the explosion, a set of experimental apparatus was designed during this investigation to simulate a large roof fall in real world. Even though it lacks geometric similitude between the experimental conditions and the real life conditions, the principle is the same. If this possibility does exist, it will justify mine authorities and safety agencies taking preventive measures when a large roof fall is known to be imminent.

3.2 TEST PARAMETERS

3.2.1. Test Loads

In real life conditions, the weight of the falling roof is dependent upon its plan area, its thickness and rock density. In the case of a totally bounded system (no leakage), it can be showed that the peak pressure developed is independent of either the plan area or the extracted height (McPherson, 1995b). The situation is somewhat different in the real condition of air displacement from the collapsing zone. The plan area of the falling roof must be large so that the reducing space under the falling material offers a significant resistance to the displacement of the air. The numerical simulation for full-scale application becomes unstable at areas of less than 20 m x 20m. Generally, the thicker the falling block, the higher the values of peak pressure. After the falling block comes to rest, the gauge pressure (absolute pressure - P_o) is simply that of the weight of the block distributed over the floor area. The plan area and the thickness of the falling block determine the dimension of the model of the simulation experiment.

The falling weight consisted of a solid steel piston and an overlying horizontal plate on which concrete slabs were placed. The diameter and the length of the solid steel piston were 102 mm (4 in) and 1.02 m (40 in), respectively. The dimension of the horizontal plate was 91cm x 91cm x

2.5cm. The size of the concrete slab was 70cm x 40cm x 7cm with a weight of 63.5 kg (140 lb) each. Figure 3.1 shows the combined test loads. This whole assembly was used to simulate the falling roof.

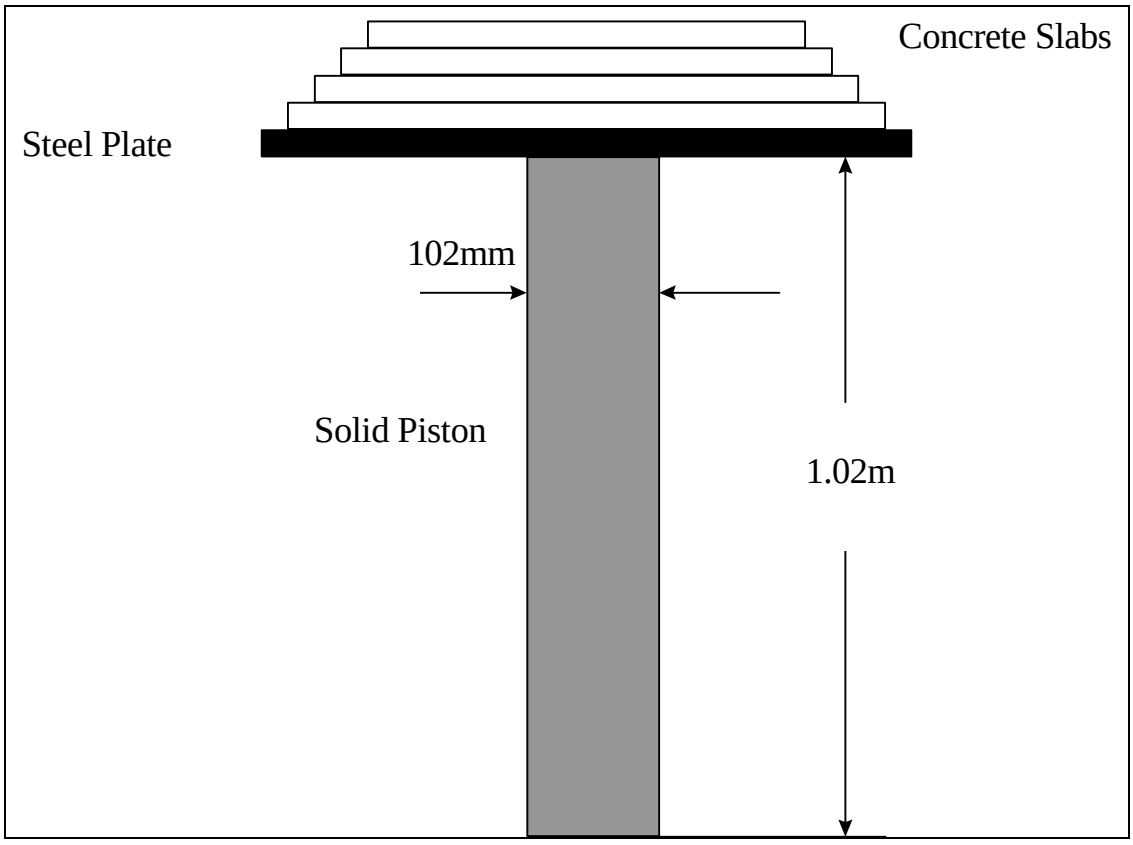

Figure 3.1. A schematic diagram of the combined test loads simulating the falling roof.

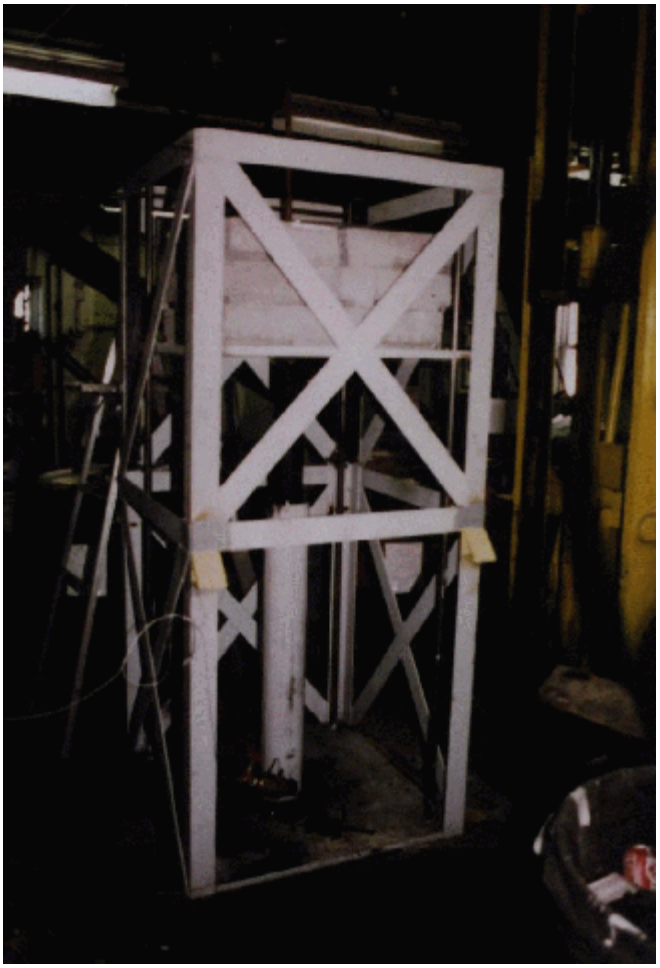

Plate 3.1. Views of the combined test loads.

During the development of the model, a series of initial trial tests were conducted with differing drop loads and using air only. This process gave experience of pressures and temperature when no chemical reaction happened. The drop rate of the loads can not be too fast or too slow. By doing the drop tests with air only repeatedly, this led to a decision to maintain the combined mass of the solid steel piston, supporting plate and concrete ballast at 600 kg (1320 lb). For the following tests with methane and/or coal dust, this combination of the test loads was maintained throughout the whole investigation. It also indicated the order of peak air pressure to be expected during a test with air only. In addition, a brass piston ring was inserted around the piston close to its bottom end. This gave excellent contact between the piston and the wall of the cylinder.

3.2.2. Cylinder

For a given plan area of the falling roof, variation in the extracted height changes the total volume of the air to be compressed and displaced from under the falling roof. Again, for the no leakage

situation, the peak pressure is independent of the height of seam extraction. For the real (leakage) case, the resistance to air displacement is greater at any given time for a smaller extraction height after the collapse commences. Hence, the air pressure builds up more rapidly and reaches a higher initial peak value than for greater extraction heights. The overall effect of extracted height on temperature behavior is somewhat limited but exhibits slightly higher rates of temperature rise for the large heights of extraction.

A steel cylinder of slightly more than 102 mm (4 in) in diameter and 0.94 m (37 in)

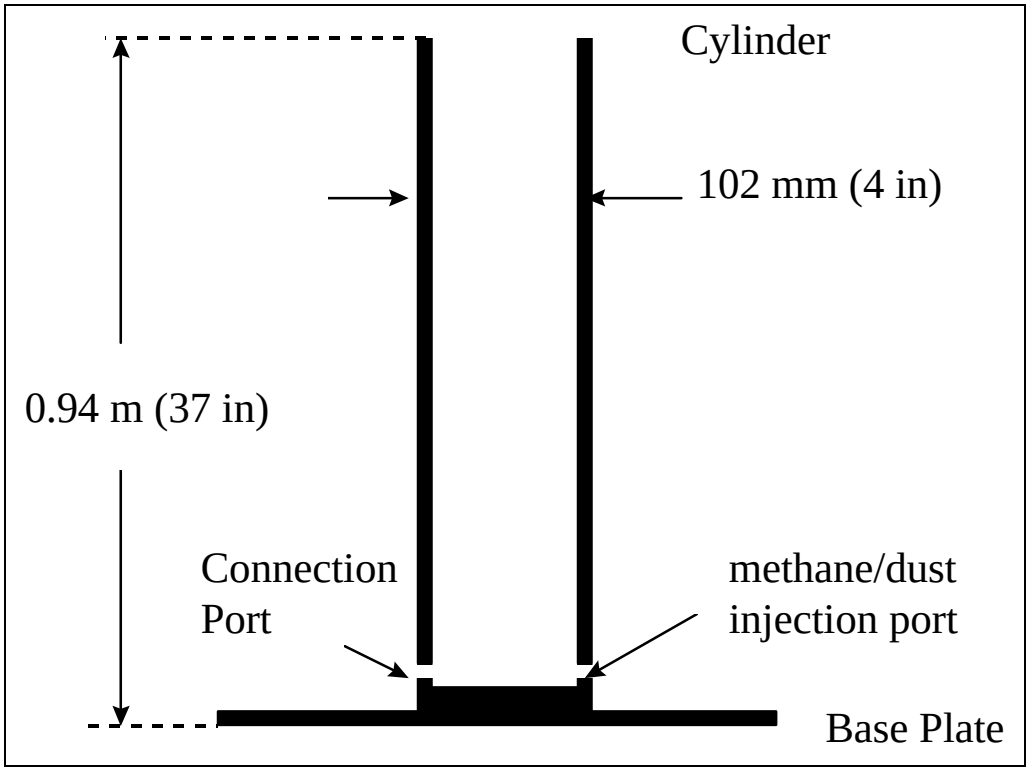

Figure 3.2. A schematic diagram of the cylinder simulating the compressed zone.

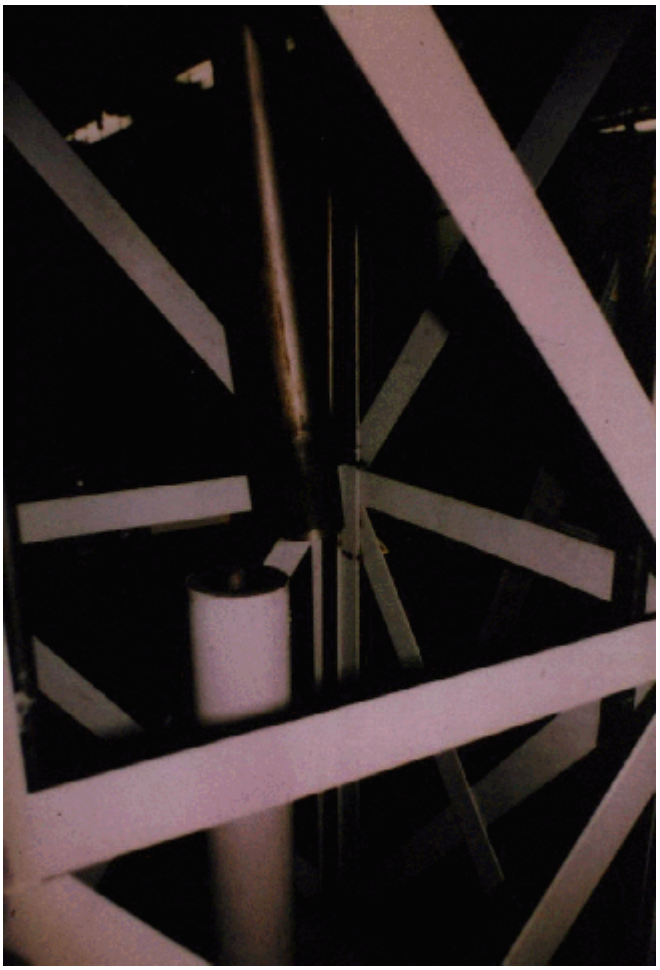

Plate 3.2. A close view of the cylinder and the piston.

Plate 3.3. A view of the cylinder.

in height was used to simulate the compression zone. In order to make the piston move smoothly inside the cylinder, a silicon-based (non-flammable) lubricant was used between the piston and the wall of the cylinder. Fig 3.2 shows a schematic diagram of the cylinder simulating the compressed zone.

3.2.3. Chamber

Underground worked-out areas are connected to entries immediately adjacent to the gob area. A brass chamber of 25 mm (1 in) diameter was connected to the bottom of the cylinder. This simulated the entries immediately adjacent to the gob area. The brass chamber opened to the outside atmosphere via an orifice. This, in turn, simulated the remainder of the mine infrastructure through to the surface opening. After testing several sizes of orifices, its final diameter was determined to be 1.6mm (0.0625 in). Figure 3.3 represents a schematic diagram of the chamber simulated the entries immediately adjacent to the gob area and the remained mine infrastructure.

3.2.4. Methane

3.2.4.1. The Nature of Methane

Since the history of mining industry, methane has been the most dangerous gas in underground mining environments. Methane is formed by bacterial and chemical action on organic material. Methane is not toxic but is particularly dangerous because it is flammable and forms an explosive mixture with air. Methane is retained within fractures, voids and

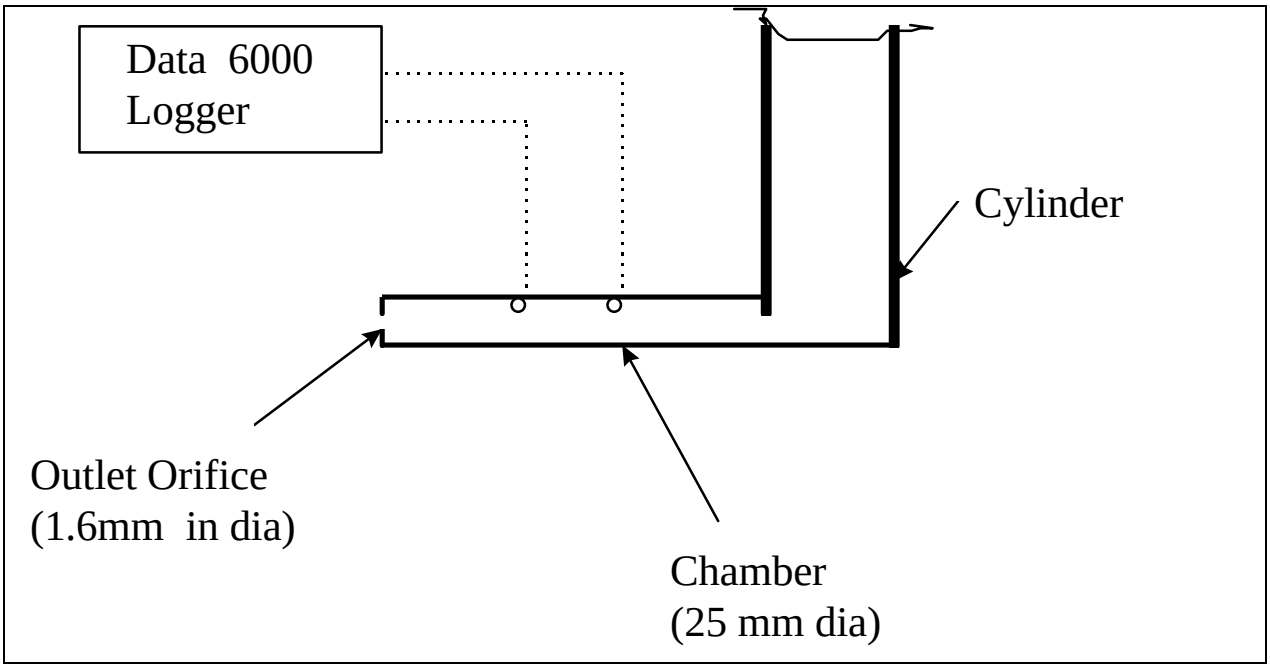

Figure 3.3. A schematic diagram of chamber simulated the entries immediately adjacent to gob area and remained mine infrastructure

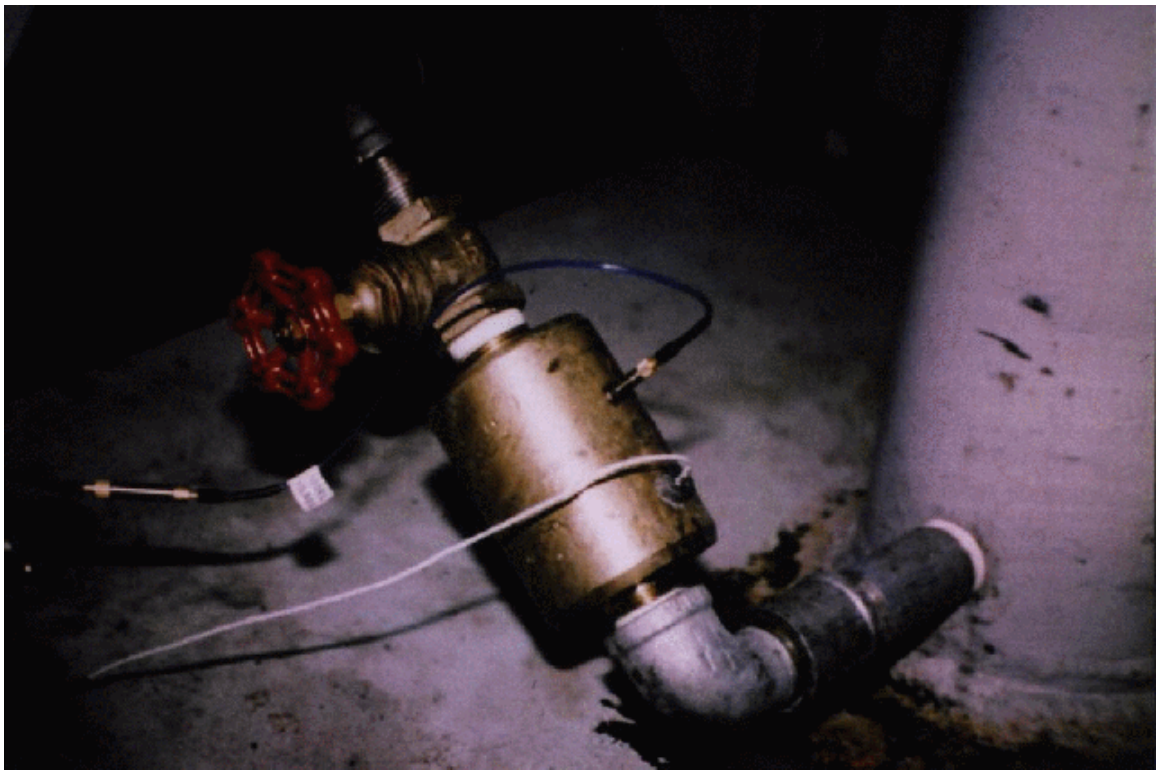

Plate 3.4. A close view of the chamber, pressure and temperature transducer.

pores in the rock either as a compressed gas or adsorbed on mineral (particularly carbon) surface. Methane itself has no odor. Its density is a little over half that of air. This gives rise to a dangerous behavior pattern - methane can form pools or layers to other emanating sources.

3.2.4.2. The Explosible Limits of Methane

From practical experience it is known that explosive gases may be rendered non-flammable, that is incapable of sustaining combustion waves, by addition of diluted gases in sufficient quantity. Such dilute may consist of excess fuel or excess oxidant or inert gases, and standardized experimental procedures are in use to determine the quantity of dilute that must be added to a fuel-oxidant mixture, or to a single-component explosive gas, to render the mixture non-flammable.

The explosible range for methane in air is normally quoted as 5% to 15%, with the most explosive mixture occurring at 9.8%. Under the normal atmosphere condition, while the lower limit remains fairly constant, the upper explosive limit reduces as the oxygen content of the air falls. The flame will propagate through the mixture within the range 5% to 14%(flammability limits). Figure 3.4 illustrates a well known diagram first produced by F. Coward in 1928. This can be used to track the flammability of air-methane mixtures as the composition varies. In zone A, the mixture is not flammable but is likely to become so if further methane is added or that part of the mine is sealed

off. In zone B, the mixture is explosive and has a minimum nose value at 12.2% oxygen. Zones C and D illustrate

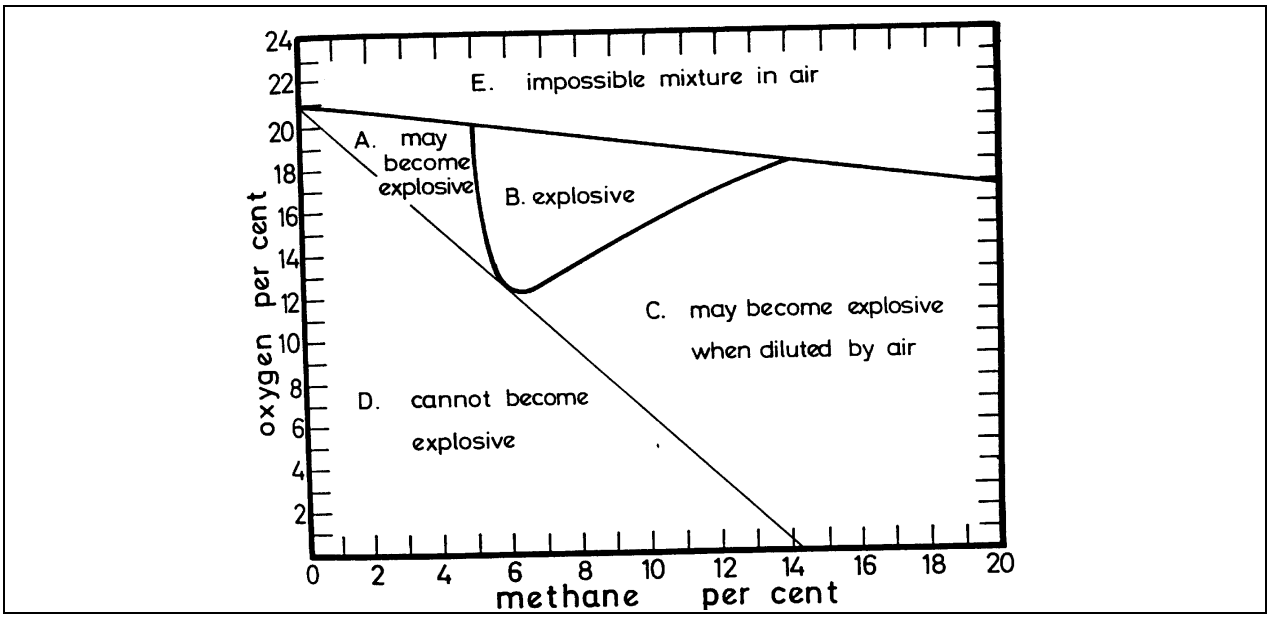

Figure 3.4. The Coward diagram for methane in air (after Coward, 1928)

mixtures that may exist in sealed areas. A mixture in zone C will become explosive if the seals are breached and the gases intermingle with incoming air. However, dilution of mixtures in zone D can be accomplished without passing through an explosive range (McPherson, 1993). Note also that as the pressure and temperature increase, the explosive limits of methane becomes a little wider (Lidin, 1964).

3.2.4.3 The methane Concentrations for the laboratory tests

In order to put methane into the cylinder, a self-made methane injector was used. Its diameter and length were 8cm and 40cm, respectively. To cover the whole explosive limits of methane, the methane concentrations of 0, 2.5, 5, 10, 15, 20 percent by volume were selected. A schematic diagram of the methane injector is illustrated in Figure 3.5.

3.2.5. Coal Dust

3.2.5.1. The Definition of Coal Dust

Coal dust, regarded from the viewpoint of its explosibility, is the name used for the fractions of comminuted coal which take part in the explosion. This is the most general definition. Coal is not,

obviously, an individual chemical compound. There are serious differences between separate seams in which coal has varying properties.

3.2.5.2. The Formation of Coal Dust in Mines

In underground coal mines, exploitation of coal seams is inseparable from the formation of coal dust. Only through underground gasification of coal is it possible to

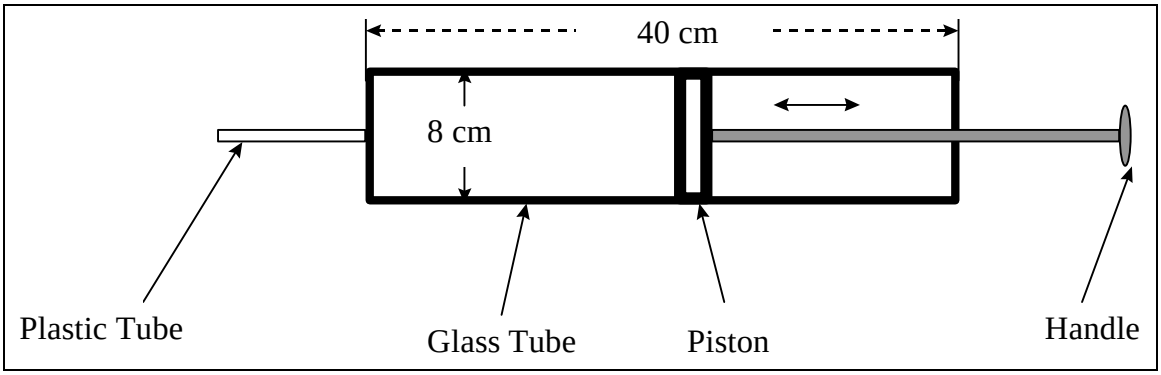

Figure 3.5. A schematic diagram of self-made methane injector.

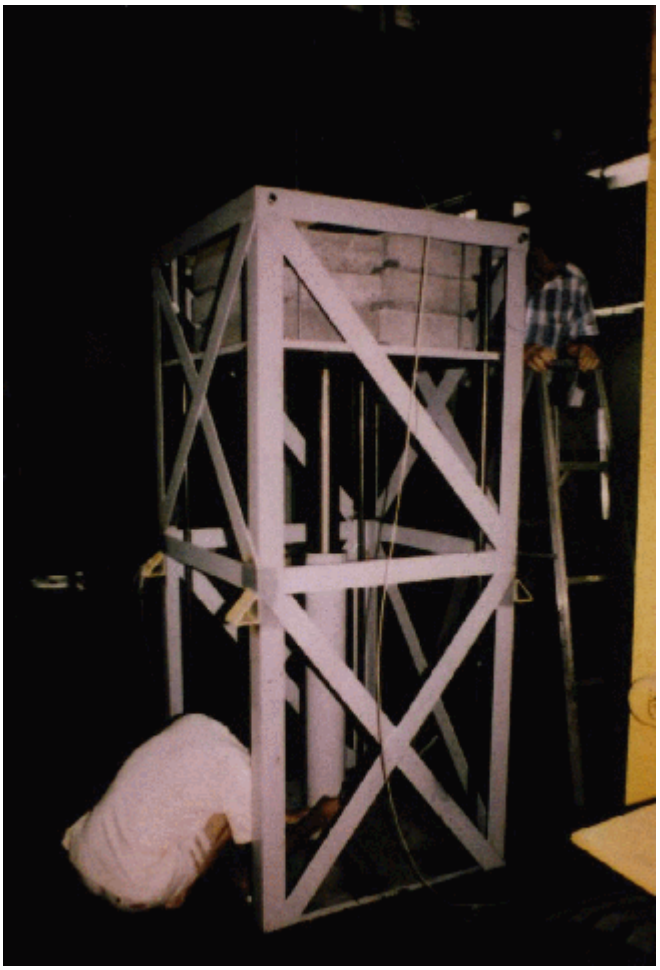

Plate 3.5. A view of injecting methane.

utilize coal seams without producing coal dust. The present way of the extraction of coal makes the formation of coal dust unavoidable. Coal dust is formed in mines in course of the winning, loading and transporting of coal. Furthermore, large quantities of coal dust are produced through the crushing of coal by the rock pressure.

3.2.5.3 Mechanism of Coal Dust Explosion

Coal dust will only explode if a supply of oxygen (oxidant) is present and a source of ignition. Ordinary combustion becomes an explosion when the rate of heat production is so great that very rapid expansion takes place or, if the expansion is restrained, rapid pressure build-up takes place. Another feature of a coal dust explosion is that the speed of the flame through the coal dust cloud is very much faster than in the case of mere combustion. It would appear that the basic condition for a coal dust explosion is when coal dust particles of small size (i.e. high relative surface area) in

a cloud are spaced far enough apart for each particle to have access to sufficient oxygen for complete combustion but close enough for heat produced by the burning of one particle to support the combustion of the next and so on.

Explosion can be divided into deflagrations and detonations. In a deflagration the shock waves travel at the speed of sound in the cloud of unburnt dust which has not yet contributed to the explosion (about 330 m/s) while the flame front follows at a slower speed. There is, therefore, a time lag between the arrival of the shock wave at a given point and the arrival of the flame, and this interval can be used to advantage in that the shock wave can be made to trigger flame quenching or venting devices which will arrest the progress of the flame or nullify the pressure build-up. In a detonation the flame front and the shock travel together at speed of sound in the gases produced by explosion (about 1000 m/s) and will thus continue until all the available dust has been consumed. Most industrial dust explosions are deflagrations with flame speeds of up to 100 m/s, and this is so because the initial energy of the igniting source is small and the scale of operation is also relatively small. In coal mines, however, the igniting source is usually an explosion in itself i.e. a methane explosion, and methane may continue to augment the effects of the dust. Conditions for detonation exist and in a fully developed coal mine dust explosion the speed of sound may be exceeded (Holden. W, 1982).

Coal dust explosions in coal mines constitute a special case in that the surfaces of the airways restrain the explosion and force it to travel along the airways. The pressure build-up is , therefore, compounded in these directions. This phenomenon is not as marked in bord and pillar workings as in concentrated longwall workings.

3.2.5.4 Ignition Sensitivity of Coal Dust

As with gas explosions there is a stoichiometric dust concentration which can be calculated and which theoretically should give the maximum flame speed. There are also upper and lower limits. The correlation between theoretical and observed phenomena is much better in the case of gases than coal dusts. The ignition sensitivity of coal dust can be expressed in terms of the minimum temperature required to create an ignition or the minimum energy required to create an ignition. In practice the two are not independent and both must be taken into account. Most coal dusts also have different ignition sensitivities depending on whether the ignition source is a spark or a hot surface, or whether the dust is in a cloud or a layer. A further related factor is the minimum dust concentration which will ignite, which in turn depends on how well dispersed the coal dust is, how turbulent the coal dust cloud is, the coal dust size distribution and the moisture content of the coal dust (Holden. W, 1982). Table 1 illustrates the typical ignitionsensitivity of coal dust.

Table 3.1. Variation of coal dust explosibility with respect to volatile content. (After Holding)

Volatile Content (%)	Minimum Ignition Temperature (^oC)		Minimum Explosible Concentration (g/m^3)
	Cloud	Layer	
12	670	240	----
25	605	210	120
43	575	180	50

3.2.5.5 Coal Dust Concentrations of Laboratory Tests

In the laboratory tests, bituminous coal dust was used. A series of amount of 0, 10, 20, 30g coal dust were injected into the cylinder by using a self-made coal dust injector. According the volume of the cylinder, the coal dust concentrations employed were 0,

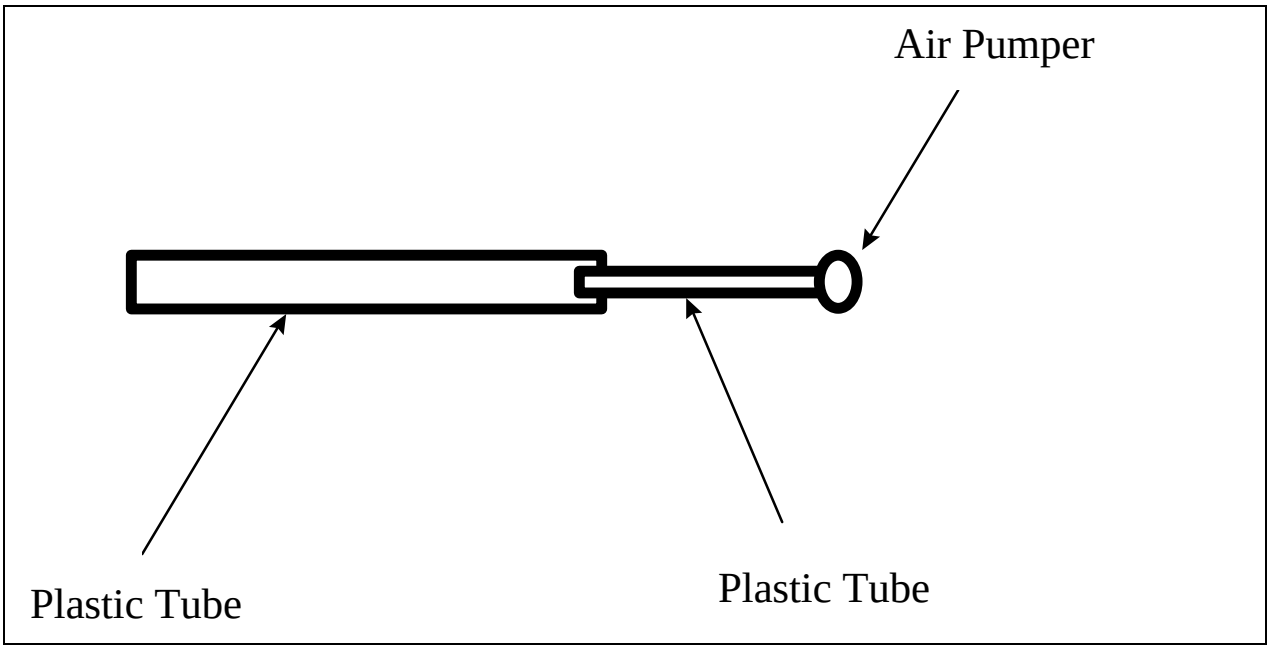

Figure 3.6. A schematic diagram of self-made coal dust injector.

Plate 3.6. A view of injecting coal dust.

1316, 2632 and 3948 g/m^3. Figure 3.6 illustrates a schematic diagram of self-made coal dust injector.

3.3 THE MONITOR SYSTEM

3.3.1 Pressure Transducer

The PCB ceramic-coated integral diaphragm ballistic pressure transducer (Model 118A) was used. It can withstand extreme flash temperatures and high overload pressures. The pressure sensitive area is permanently coated with ceramic to thermally insulate against destructive flash temperature effects. Table 3.2 indicates some parameters of this Model.

Note also that the Model 118A pressure transducer needs to be used with a charge amplifier and 482A06 line powered signal conditioners. The transducer's response interval is 5 ms. The output signal of the pressure, in milli-votage, was monitored and recorded using a DATA 6000 data logger. It needed to be calibrated to the standard pressure units, psi or Pa.

3.3.2 Temperature Sensor

The 100W30 Platinum Resistance Temperature Detector was used to monitor the variance of temperature inside the cylinder. It utilizes a thick film design for long term stability. Table 3.3 indicates the main technical data of the RTD.

Table 3.2. Specification of Model 118A (anon, 1993).

Range	psi	80,000
Maximum Pressure	psi	100,000
Resolution	psi	2
Sensitivity (nominal)	pC/psi	0.10
Resonant Frequency	kHz	300
Rise Time	usec	2
Linearity (best straight line)	%	2
Polarity		Negative
Insulation Resistance	ohms	$1x10^{12}$
Capacitance	pF	5
Acceleration Sensitivity	psi/g	0.01
Temperature Coefficient	$\%/^{o}F$	0.01
Temperature Range	^{o}F	± 400
Flash Temperature	^{o}F	4,000
Vibration; Shock	g's peak	10,000; 20,000

Table 3.3. The Main technical data of the Resistance Temperature Detector (anon, 1991).

Sensor Type	Thick film platinum RTD
Surface Insulation	1000 M ohm at room temperature and 250 V, or 50M ohm at 600^{o}C and 50V
Response Time	Less than 0.1 sec to reach 63% of ultimate temperature
Self Heating Effect	Less than 0.006^{o}C/mw
Stability after Temperature Cycling	Less than 0.05% after 10 cycles between -70 and 600 ^{o}C
Temperature Range	-70 to 600 ^{o}C
Fundamental Interval	38.5 ohms nominal (0 to 100^{o}C)
Normal Resistance	100 ohms at 0^{o}C

Unfortunately, the Resistance Temperature Detector was much slower, having a response time of 250 ms. This could not give a quick response to the temperature trend during the tests. An RTD with faster response was too expensive. The output signal of the temperature, in milli-voltage, was also monitored and recorded using the DATA 6000. And then, it was converted to the standard temperature scale (^{o}C).

3.3.3. The DATA 6000 Logger

3.3.3.1. <u>The General Description of DATA 6000</u>

The DATA 6000 is a portable data waveform analysis instrument, designed for table-top use with a “flip” stand for convenient viewing. It is equipped with integral carrying handles, and the overall dimensions are compatible with a standard 19-inch rack-and-panel mounting, The instrument is designed to accept any one of a number of available plug-in front-end modules, through which multiple analog inputs are acquired at user-selected sampling speeds, and through which the digitized signals are transferred to main frame data storage for subsequent processing and display. It applies an extensive library of pre-programmed analysis functions to the stored data; and displays the signals and/or the processed information on a large (9’’-diagonal) screen. Plotter and floppy disky peripherals options provide hardcopy recordings of waveform data, and non-volatile storage of waveform data, control setups, and programs (Allis-Chalmers, 1985).

3.3.3.2. <u>The Setup of DATA 6000</u>

The signals of the pressure transducer were input to the Channel One of DATA 6000 while the signals of RTD were input to the Channel Two. The sampling rate was one point every 5 ms. The trigger came from the Channel One with its threshold level 15 mv. After each test, data was saved to floppy disk from the buffer of the DATA 6000.

3.3.3.3. The Calibration of the Pressure Signals

The voltage signals of the pressure collected by the DATA 6000 need to be converted to the pressure units. Fig 3.7 indicates the calibration curve of the PCB Piezotronics.

3.3.3.4 The Calibration of the Temperature Signals

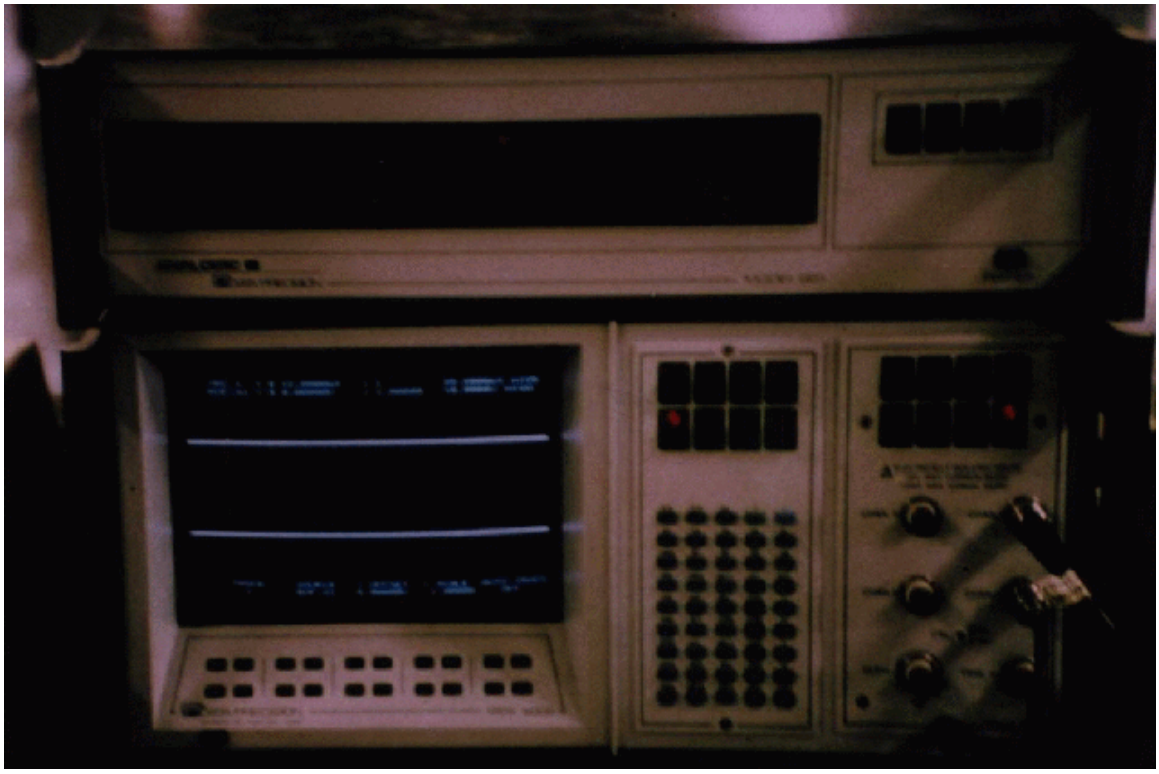

Plate 3.7. A close view of the DATA 6000 logger.

The voltage signals of the temperature recorded by the DATA 6000 was converted to the standard temperature scale (^{o}C). Fig 3.8 shows the typical calibration chart for the temperature sensor.

3.3.3.5 The Combination of the Monitor System

The pressure transducer and temperature detector were located in the middle of the chamber. The pressure transducer was connected to the charge amplifier, capacitor, power supply and channel one of DATA 6000 in that order, while the resistance temperature detector was connected to thermometer and channel two of the DATA 6000 in that order. Fig 3.9 indicates the connection diagram of the monitor system.

3.4. THE FINAL MODEL OF LABORATORY TESTS

After a series of trial tests, a final model of laboratory tests was determined. Fig 3.10 is a schematic diagram of this model.

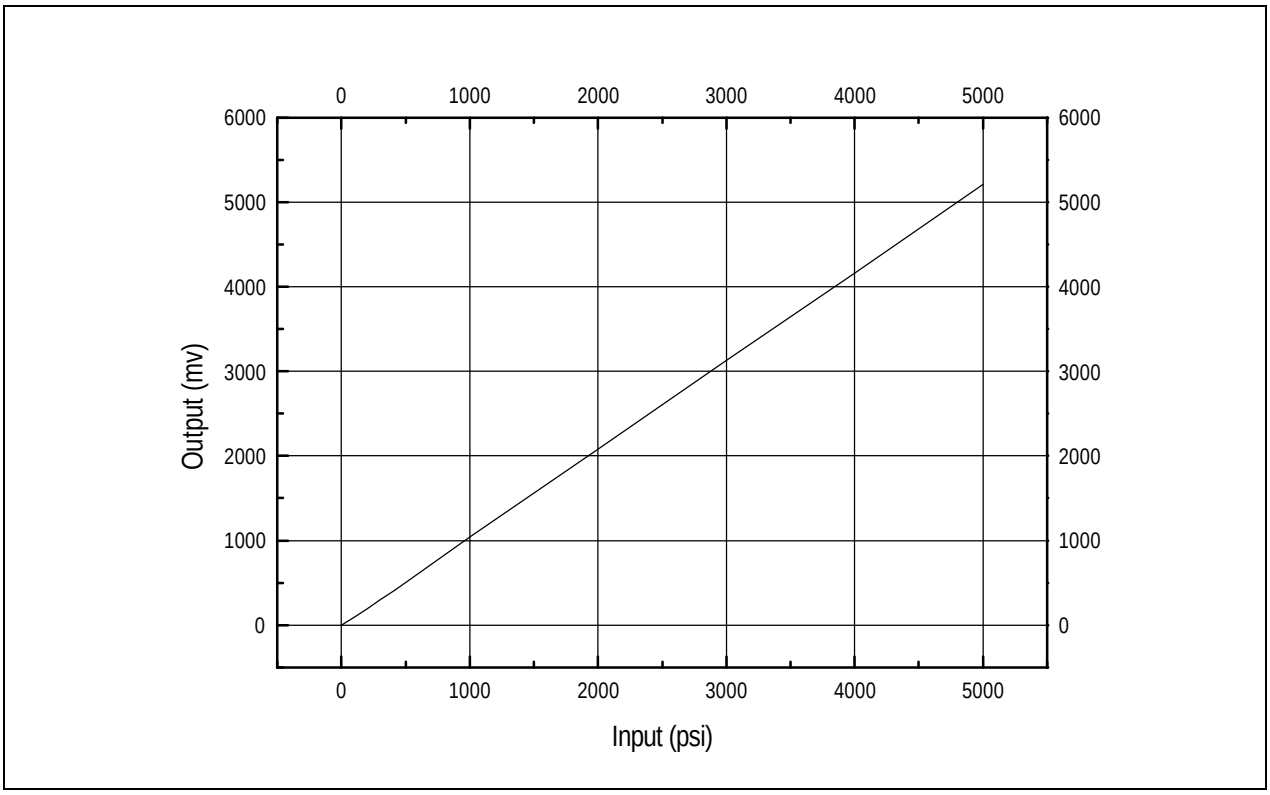

Fig 3.7. PCB Piezotronics' calibration curve.

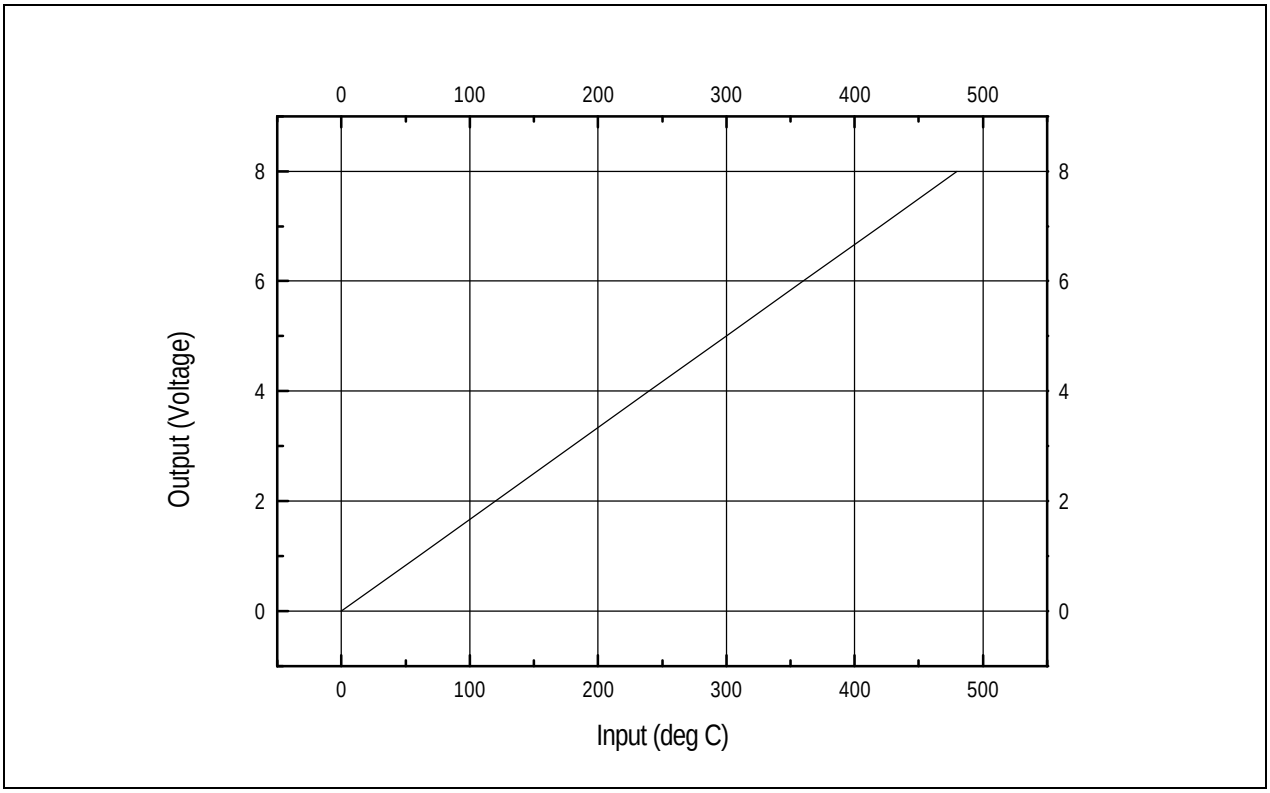

Fig 3.8. The typical calibration chart for the temperature sensor.

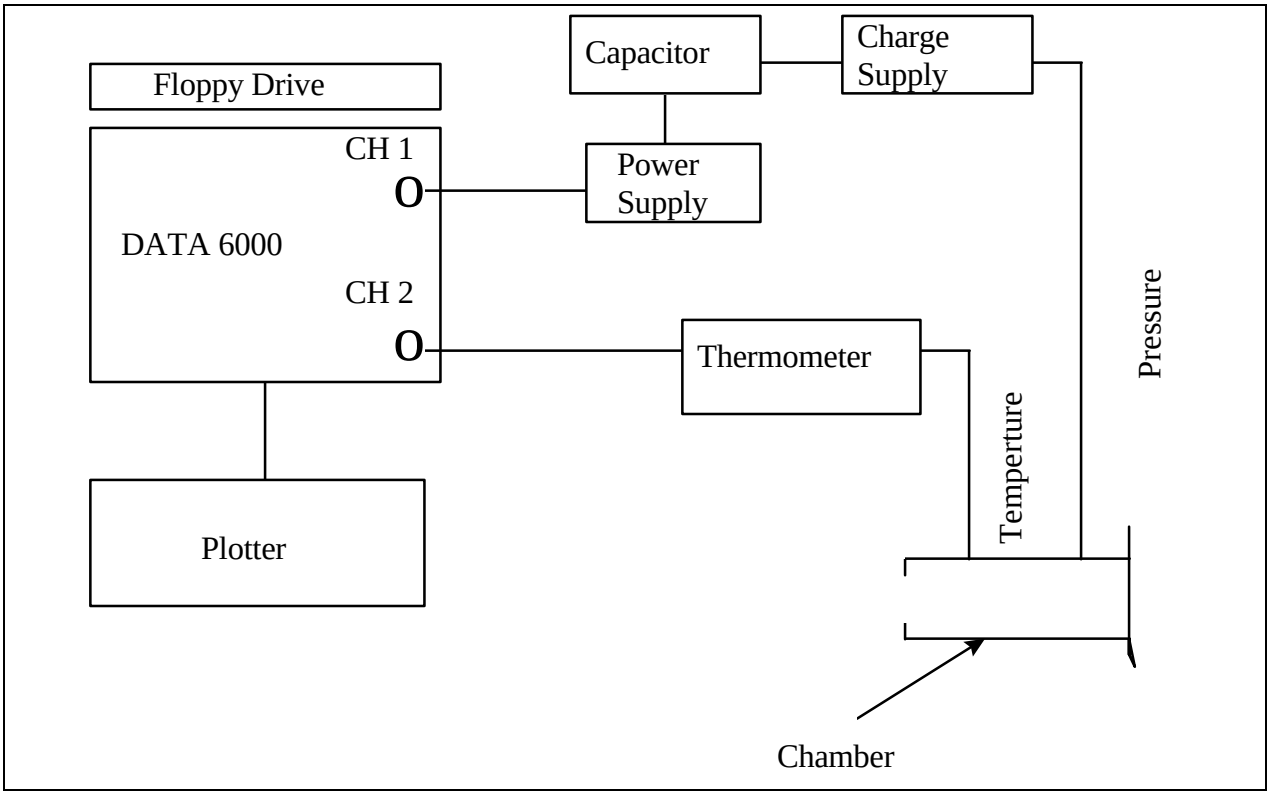

Fig 3.9. A schematic connection diagram of the monitor system.

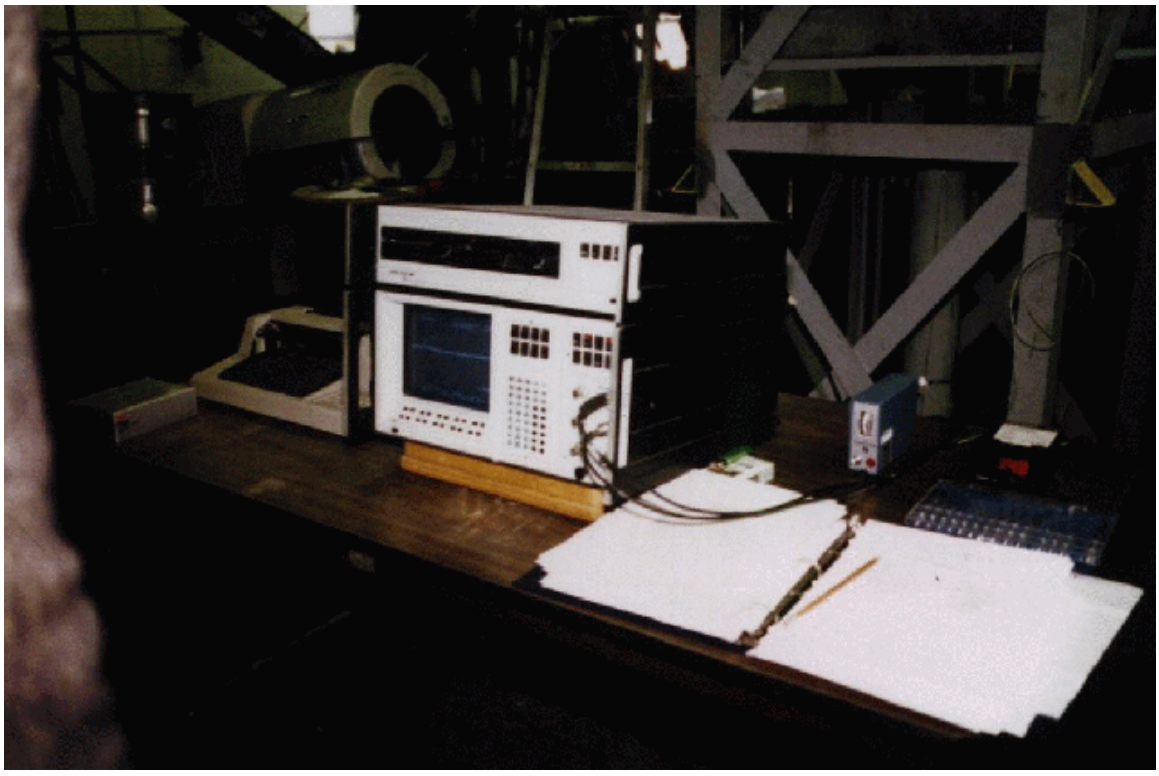

Plate 3.8. A close view of the monitoring system.

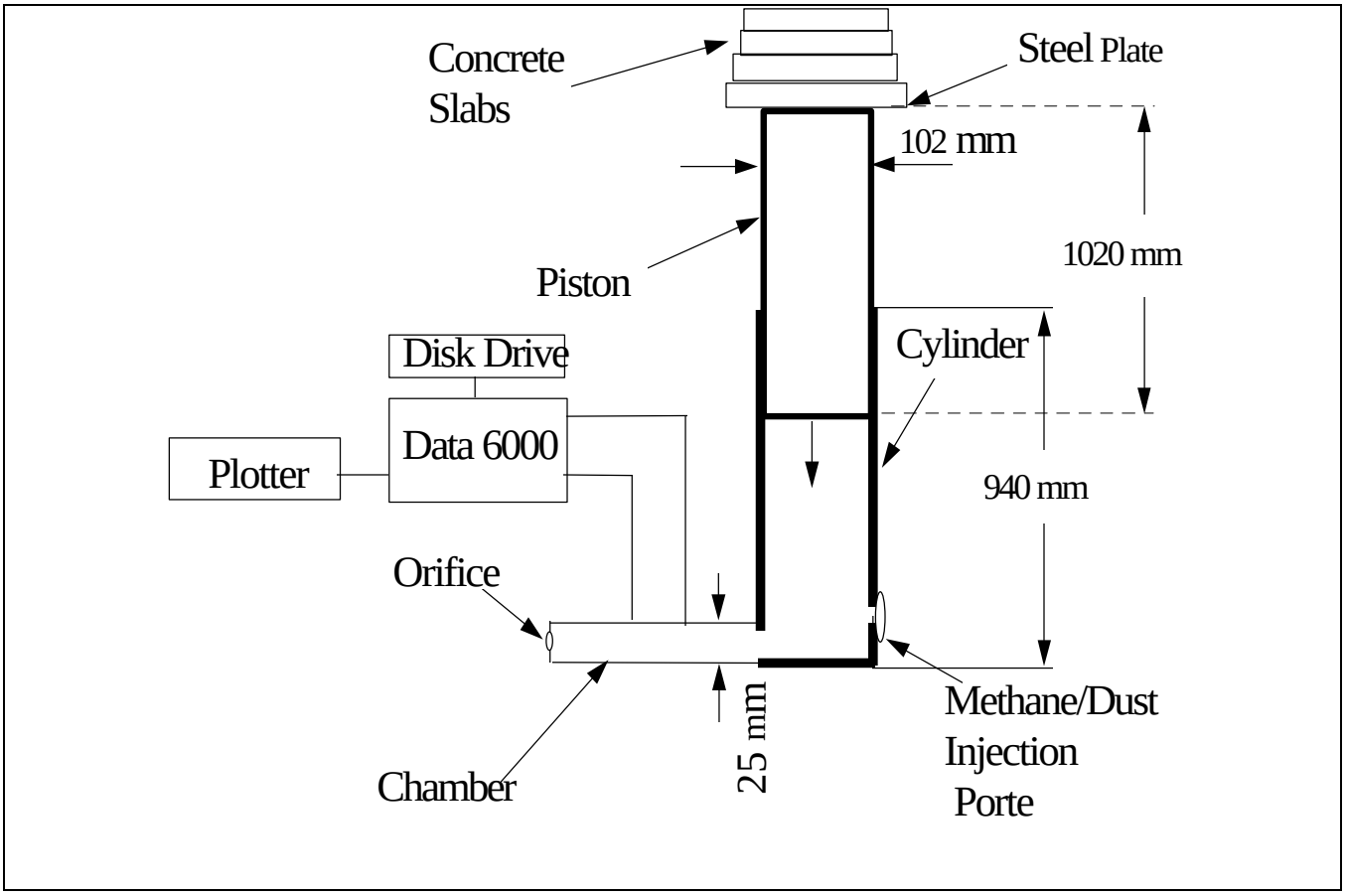

Fig 3.10. A schematic diagram of laboratory tests assembly.

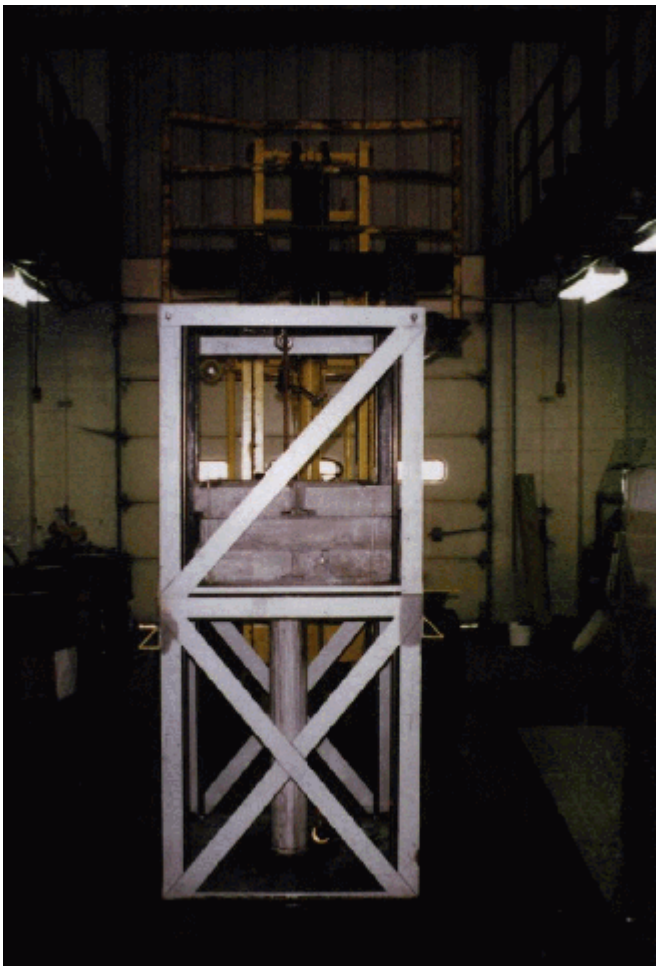

Plate 3.9. A view of the whole test assembly.

Chapter 4. Results

This chapter will review the procedures employed and the results obtained for the laboratory experiments. Since the drop-test assembly used for these experiments was specifically constructed for them it is appropriate to cover the start-up testing prior to a discussion on the results from the intended studies.

Such an approach is relevant for two reasons: (1) it validates the original design, (2) it will be useful in determining the actual conditions employed during the drop-test to follow.

4.1. THE START-UP TESTING

The start-up testing was mainly conducted on the two test elements: test loads and the size of the orifice. For the other parameters, such as drop height, chamber diameter and cylinder diameter, an initial run gave an impression that this system would work. By doing drop-tests repeatedly with air only, six the concrete slabs (with a total ballast at 600 kg (1320 lb)) were reasonable for the experiments to follow. Three different diameters of the orifice, which were 1.6 mm (0.0625 inch), 3.2mm (0.125 inch) and 4.8mm (0.1875 inch), were tried. The latter two diameters were so large that the piston came to rest very fast. Finally, the diameter of the orifice simulating the immediately entries adjacent the gob area was determined to be 1.6 mm (0.0625 inch).

4.2. TEST PROCEDURES

For the subsequent test, the drop loads and height, diameters of chamber and cylinder and the size of the orifice remained unchanged. The variables were the content of coal dust and methane. Each drop test was conducted by the procedure outlined below:

1) Clean up the coal dust in the chamber and cylinder from the last test.
2) Connect the pressure transducer with the charge supply, capacitor, power supply and channel 1 of the DATA 6000 in that order. Also place the temperature sensor, thermometer and channel 2 of the DATA 6000 together.
3) Connect floppy drive and plotter to the DATA 6000.
4) In order to ensure that the air, gas and coal dust were well mixed, the methane and/or coal dust were drawn through the injection port at the base of the cylinder while the piston was being lifted to its uppermost position. The drop loads were lifted by the fork truck.
5) Seal the injection port.
6) Set the trigger value (15 mv) the sampling interval (5 ms) and the sampling points (1000 points on the data logger). Record instrument was ready.
7) Mount the orifice cap.
8) Release quickly the loaded piston (Plate 4.1).
9) Plot out the pressure and temperature curves (Fig 4.1, Fig 4.2).

10) Write down the tests parameters on the data collection sheet (Table 4.1).

Each test followed the above procedure cycle. In some situations, the broken temperature sensor needed to be replaced.

Plate 4.1. A view at the moment of releasing the piston.

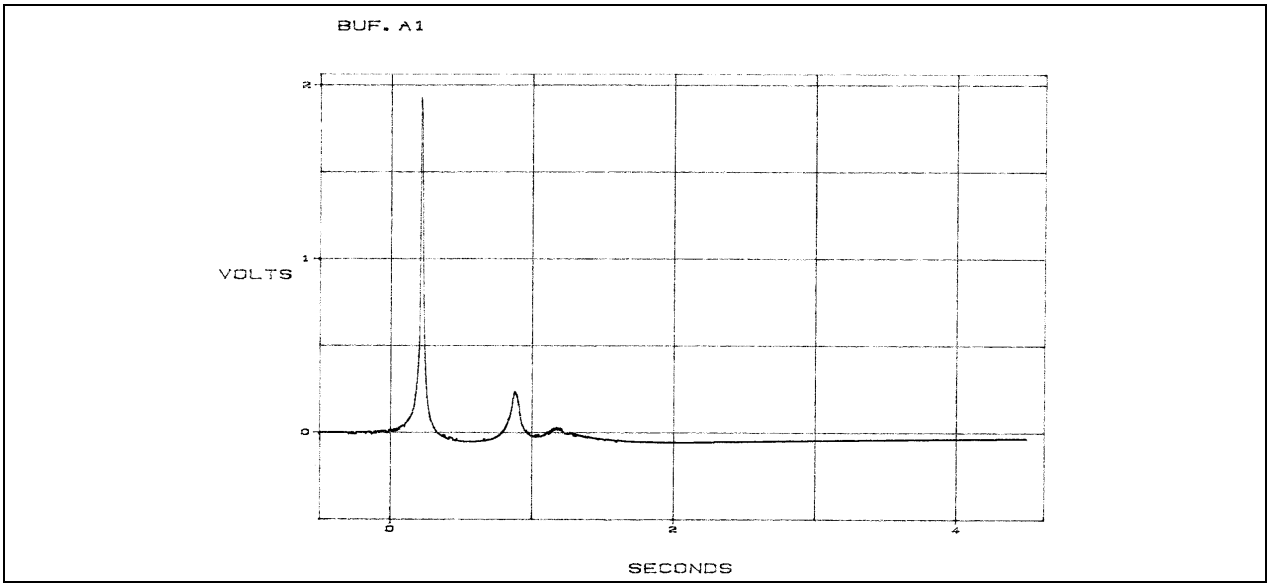

Fig 4.1. Variation of air pressure during a laboratory test.

Plate 4.2. A view of printing out pressure profile.

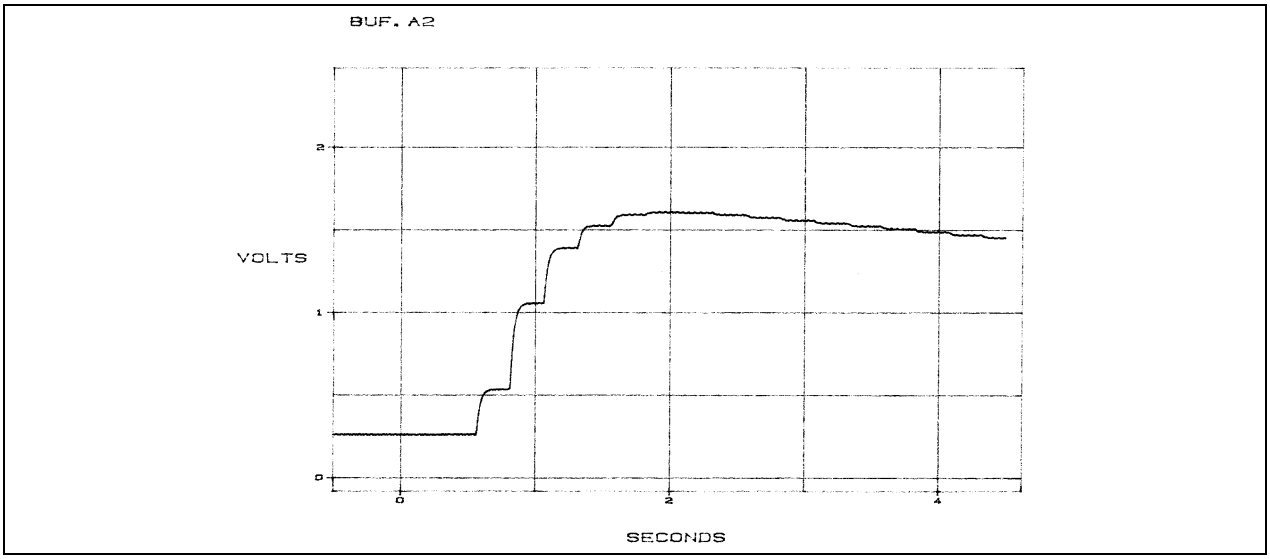

Fig 4.2. Variation of air temperature during a laboratory test.

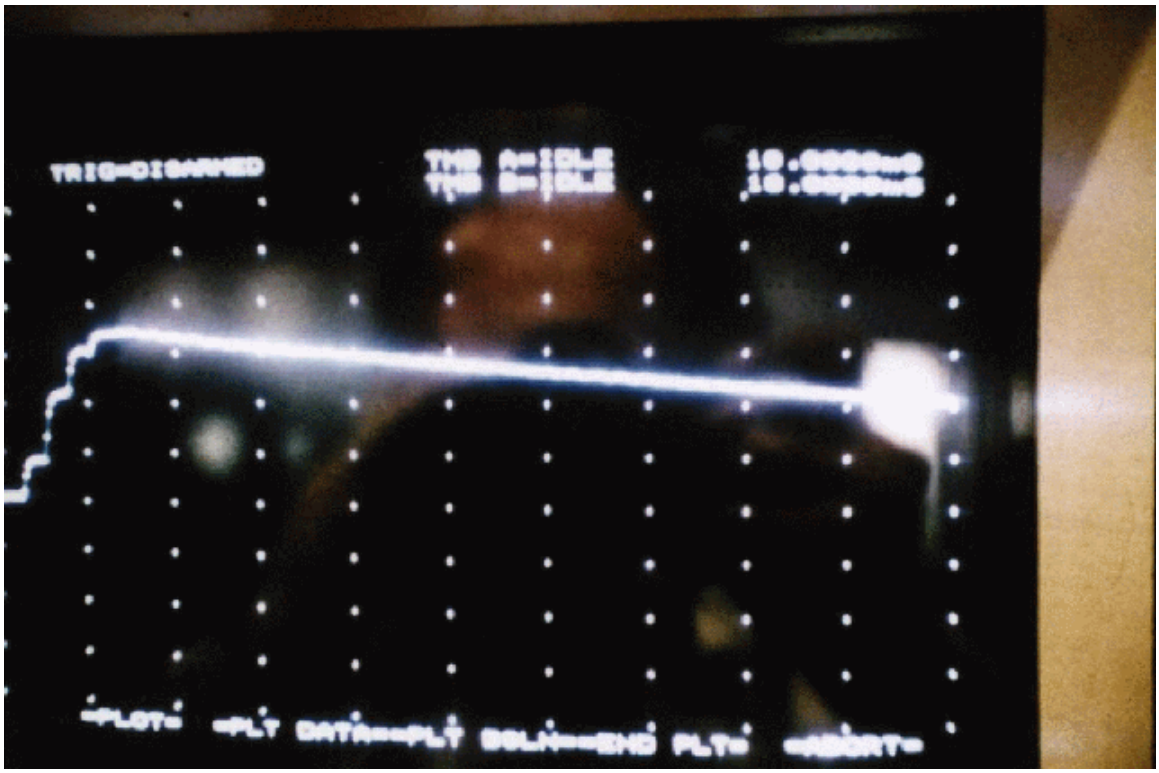

Plate 4.2. A close view of temperature profile.

Table 4.1. The Tests Parameters Data Collection Sheet.

Data for Compression Test of Air

Test Date:_____ Test No:_____

Time:_____ Name:_____

Dust Load (g):_____ Peak Pressure (kPa):_____

Load on Rig (kg):_____ Time (ms):_____

Drop Height (m):_____ Initial Temperature (^{o}C):____

Leakage Diameter (mm):_____ Average Temperature Record (^{o}C):_____

Methane Concentration (%): Times of Bouncing:_____

Description:

4.3 THE TRANSFORMATION OF TEST DATA

The voltage signals collected by DATA 6000 need to be transferred to the standard units of pressure (kPa) and temperature (^{o}C). Because the temperature sensor could not promptly response to the actual variation of the temperature inside the cylinder, it seemed to be of limited use in the precise analysis of the laboratory results. Nevertheless, it indicated a continuously rising pattern as predicted by the computer simulations. Because of format incompatibility, the data stored on the DATA 6000 could not directly be inputted to computer. It needed to be calculated and entered manually. This was a time - consuming task. The laboratory tests were run for a variety of combinations of methane and coal dust. Table 4.2 gives the test schedule matrix. A typical transformation of the pressure is given in Table 4.3. Because the pressure output signals are proportional to the pressure and inversely proportional to the temperature, some points on the pressure curves have negative values. Compared with high peak pressure, the negative effects of temperature on the pressure signals are much smaller and could be ignored.

Table 4.2. The test schedule matrix.

Methane **Coal Dust**	**0 %** **by volume**	**2.5**	**5**	**10**	**15**	**20**
0 (g/m^3)						
1316						
2632						
3948						

Table 4.3. A typical data transformation from DATA 6000.

Time (s)	Press (mv)	Press (kPa)	Time (s)	Press (mv)	Press (kPa)	Time (s)	Press (mv)	Press (kPa)
0	0	0	0.295	13.131	90.538	0.495	887.25	6117.6
0.1	1.25	8.619	0.3	13.756	94.848	0.5	846.61	5837.4
0.105	1.875	12.928	0.305	14.381	99.157	0.505	664.66	4582.8
0.11	1.876	12.935	0.31	15.01	103.49	0.51	431.43	2974.7
0.115	1.876	12.935	0.315	16.257	112.09	0.515	290.75	2004.7
0.12	1.876	12.935	0.32	16.882	116.4	0.52	210.09	1448.6
0.125	1.876	12.935	0.325	18.133	125.03	0.525	159.44	1099.4
0.13	1.876	12.935	0.33	19.383	133.65	0.53	124.43	857.9
0.135	1.876	12.935	0.335	20.01	137.97	0.535	103.17	711.36
0.14	1.876	12.935	0.34	21.259	146.58	0.54	83.161	573.39
0.145	1.876	12.935	0.345	23.135	159.52	0.545	68.154	469.92
0.15	1.876	12.935	0.35	24.385	168.13	0.55	56.274	388.01
0.155	3.126	21.554	0.355	26.261	181.07	0.555	48.146	331.97
0.16	3.126	21.554	0.36	27.512	189.7	0.56	40.017	275.92
0.165	3.126	21.554	0.365	29.388	202.6	0.565	33.764	232.8
0.17	3.126	21.554	0.37	31.889	219.87	0.57	30.013	206.94
0.175	3.752	25.87	0.375	34.39	237.12	0.575	25.011	172.45
0.18	3.752	25.87	0.38	36.891	254.36	0.58	21.884	150.89
0.185	4.377	30.179	0.385	39.392	271.61	0.585	18.133	125.03
0.19	4.377	30.179	0.39	42.518	293.16	0.59	16.257	112.09
0.195	4.377	30.179	0.395	46.27	319.03	0.595	13.131	90.538
0.2	5.002	34.489	0.4	50.021	344.89	0.6	11.88	81.913
0.205	5.002	34.489	0.405	54.398	375.07	0.605	10.004	68.978
0.21	5.627	38.798	0.41	59.4	409.56	0.61	8.129	56.049
0.215	5.627	38.798	0.415	65.028	448.37	0.615	7.503	51.733
0.22	5.627	38.798	0.42	72.531	500.1	0.62	5.627	38.798
0.225	6.253	43.114	0.425	80.034	551.83	0.625	4.377	30.179
0.23	6.878	47.424	0.43	89.413	616.5	0.63	3.126	21.553
0.235	6.878	47.424	0.435	100.04	689.79	0.635	1.876	12.935
0.24	6.878	47.424	0.44	112.55	776.03	0.64	1.876	12.935
0.245	7.503	51.733	0.445	126.93	875.18	0.645	1.251	8.626
0.25	8.129	56.049	0.45	143.81	991.58	0.65	0.625	4.309
0.255	8.129	56.049	0.455	164.45	1133.9	0.655	0	0
0.26	8.754	60.359	0.46	190.71	1314.9	0.66	-0.625	-4.309
0.265	9.379	64.668	0.465	224.47	1547.7	0.665	-1.251	-8.626
0.27	10.004	68.978	0.47	267.61	1845.2	0.67	-1.251	-8.626
0.275	10.63	73.294	0.475	325.76	2246.1	0.675	-1.876	-12.93
0.28	10.63	73.294	0.48	408.3	2815.2	0.68	-1.876	-12.93

Time (s)	Press (mv)	Press (kPa)	Time (s)	Press (mv)	Press (kPa)	Time (s)	Press (mv)	Press (kPa)
0.695	-1.876	-12.93	0.91	174.5	1202.8	1.125	-0.625	-4.309
0.7	-1.876	-12.93	0.915	193.2	1332.2	1.13	-3.752	-25.87
0.705	-1.876	-12.93	0.92	196.3	1353.7	1.135	-5.002	-34.489
0.71	-2.501	-17.24	0.925	171.3	1181.3	1.14	-7.503	-51.73
0.715	-1.876	-12.93	0.93	141.3	974.33	1.145	-8.754	-60.359
0.72	-1.876	-12.93	0.935	110.1	758.79	1.15	-10.63	-73.29
0.725	-1.251	-8.626	0.94	83.16	573.39	1.155	-11.25	-77.6
0.73	-1.251	-8.626	0.945	63.15	435.43	1.16	-11.88	-81.91
0.735	-0.625	-4.309	0.95	48.77	336.28	1.165	-12.505	-86.222
0.74	-0.625	-4.309	0.955	39.39	271.61	1.17	-12.505	-86.222
0.745	0	0	0.96	31.26	215.56	1.175	-15.006	-103.46
0.75	0.625	4.309	0.965	26.26	181.07	1.18	-16.257	-112.09
0.755	1.251	8.626	0.97	21.26	146.58	1.185	-17.507	-120.71
0.76	1.251	8.626	0.975	17.51	120.71	1.19	-17.507	-120.71
0.765	1.876	12.93	0.98	15.63	107.78	1.195	-18.758	-129.34
0.77	3.126	21.55	0.985	14.38	99.16	1.2	-19.383	-133.65
0.775	4.377	30.18	0.99	13.13	90.54	1.205	-20.634	-142.27
0.78	5.002	34.49	0.995	11.88	81.91	1.21	-21.259	-146.58
0.785	5.627	38.8	1	11.88	81.91	1.215	-21.884	-150.89
0.79	6.878	47.42	1.005	10	68.98	1.22	-21.884	-150.89
0.795	8.129	56.05	1.01	10.63	73.29	1.225	-21.884	-150.89
0.8	9.379	64.67	1.015	10	68.98	1.23	-22.51	-155.21
0.805	10.63	73.29	1.02	10.63	73.29	1.235	-22.51	-155.21
0.81	11.88	81.91	1.025	10.63	73.29	1.24	-22.51	-155.21
0.815	14.38	99.16	1.03	10.63	73.29	1.245	-23.135	-159.52
0.82	15.63	107.78	1.035	11.88	81.91	1.25	-23.135	-159.52
0.825	17.5	120.71	1.04	12.51	86.22	1.255	-22.51	-155.21
0.83	20.1	137.96	1.045	14.38	99.16	1.26	-23.135	-159.52
0.835	22.51	155.21	1.05	14.38	99.16	1.265	-22.51	-155.21
0.84	25.64	176.76	1.055	16.88	116.4	1.27	-23.135	-159.52
0.845	28.76	198.31	1.06	16.88	116.4	1.275	-23.135	-159.52
0.85	32.51	224.18	1.065	18.13	125	1.28	-23.135	-159.52
0.855	36.89	254.36	1.07	18.76	129.3	1.285	-23.135	-159.52
0.86	41.89	288.85	1.075	20.1	137.9	1.29	-23.135	-159.52
0.865	48.15	331.97	1.08	21.26	146.6	1.295	-23.135	-159.52
0.87	54.39	375.07	1.085	22.51	155.2	1.3	-23.135	-159.52
0.875	62.53	431.12	1.09	24.39	168.1	1.305	-23.135	-159.52
0.88	71.91	495.79	1.095	26.26	181.1	1.31	-23.135	-159.52
0.885	84.41	582.01	1.1	26.26	181.1	1.315	-23.135	-159.52
0.89	97.54	672.55	1.105	21.26	146.6	1.32	-23.135	-159.52
0.895	114.4	788.95	1.11	15.63	107.8	1.325	-23.135	-159.52

Time (s)	Press (mv)	Press (kPa)	Time (s)	Press (mv)	Press (kPa)	Time (s)	Press (mv)	Press (kPa)
0.89	97.54	672.55	1.105	21.26	146.6	1.32	-23.135	-159.52
0.895	114.4	788.95	1.11	15.63	107.8	1.325	-23.135	-159.52
0.9	133.2	918.28	1.115	10.63	73.29	1.33	-23.135	-159.52
0.905	153.2	1056.2	1.12	4.38	30.18	1.335	-23.135	-159.52
1.34	-23.135	-159.52	1.555	-21.88	-150.89	1.77	-20.01	-137.96
1.345	-23.135	-159.52	1.56	-21.88	-150.89	1.775	-20.01	-137.96
1.35	-23.135	-159.52	1.565	-21.88	-150.89	1.78	-20.01	-137.96
1.355	-23.135	-159.52	1.57	-21.88	-150.89	1.785	-20.01	-137.96
1.36	-23.135	-159.52	1.575	-21.88	-150.89	1.79	-20.01	-137.96
1.365	-23.135	-159.52	1.58	-21.88	-150.89	1.795	-20.01	-137.96
1.37	-23.135	-159.52	1.585	-21.88	-150.89	1.8	-20.01	-137.96
1.375	-22.51	-155.21	1.59	-21.88	-150.89	1.805	-20.01	-137.96
1.38	-22.51	-155.21	1.595	-21.88	-150.89	1.81	-20.01	-137.96
1.385	-22.51	-155.21	1.6	-21.26	-146.58	1.815	-20.01	-137.96
1.39	-22.51	-155.21	1.605	-21.26	-146.58	1.82	-20.01	-137.96
1.395	-22.51	-155.21	1.61	-21.26	-146.58	1.825	-20.01	-137.96
1.4	-22.51	-155.21	1.615	-21.26	-146.58	1.83	-20.01	-137.96
1.405	-22.51	-155.21	1.62	-21.26	-146.58	1.835	-20.01	-137.96
1.41	-22.51	-155.21	1.625	-21.26	-146.58	1.84	-20.01	-137.96
1.415	-22.51	-155.21	1.63	-21.26	-146.58	1.845	-20.01	-137.96
1.42	-22.51	-155.21	1.635	-21.26	-146.58	1.85	-20.01	-137.96
1.425	-22.51	-155.21	1.64	-21.26	-146.58	1.855	-20.01	-137.96
1.43	-22.51	-155.21	1.645	-21.26	-146.58	1.86	-20.01	-137.96
1.435	-22.51	-155.21	1.65	-21.26	-146.58	1.865	-20.01	-137.96
1.44	-22.51	-155.21	1.655	-21.26	-146.58	1.87	-20.01	-137.96
1.445	-22.51	-155.21	1.66	-21.26	-146.58	1.875	-19.38	-133.65
1.45	-22.51	-155.21	1.665	-21.26	-146.58	1.88	-19.38	-133.65
1.455	-22.51	-155.21	1.67	-21.26	-146.58	1.885	-19.38	-133.65
1.46	-22.51	-155.21	1.675	-20.63	-142.27	1.89	-19.38	-133.65
1.465	-22.51	-155.21	1.68	-20.63	-142.27	1.895	-19.38	-133.65
1.47	-22.51	-155.21	1.685	-20.63	-142.27	1.9	-19.38	-133.65
1.475	-22.51	-155.21	1.69	-20.63	-142.27	1.905	-19.38	-133.65
1.48	-22.51	-155.21	1.695	-20.63	-142.27	1.91	-19.38	-133.65
1.485	-22.51	-155.21	1.7	-20.63	-142.27	1.915	-19.38	-133.65
1.49	-22.51	-155.21	1.705	-20.63	-142.27	1.92	-19.38	-133.65
1.495	-21.88	-150.89	1.71	-20.63	-142.27	1.925	-19.38	-133.65
1.5	-21.88	-150.89	1.715	-20.63	-142.27	1.93	-19.38	-133.65
1.505	-21.88	-150.89	1.72	-20.63	-142.27	1.935	-19.38	-133.65
1.51	-21.88	-150.89	1.725	-20.63	-142.27	1.94	-19.38	-133.65
1.515	-21.88	-150.89	1.73	-20.63	-142.27	1.945	-19.38	-133.65
1.52	-21.88	-150.89	1.735	-20.63	-142.27	1.95	-19.38	-133.65

Time (s)	Press (mv)	Press (kPa)	Time (s)	Press (mv)	Press (kPa)	Time (s)	Press (mv)	Press (kPa)
1.985	-18.76	-129.34	2.2	-17.51	-120.71	2.415	-16.88	-116.4
1.99	-18.76	-129.34	2.205	-17.51	-120.71	2.42	-16.88	-116.4
1.995	-18.76	-129.34	2.21	-17.51	-120.71	2.425	-16.88	-116.4
2	-18.76	-129.34	2.215	-17.51	-120.71	2.43	-16.88	-116.4
2.005	-18.76	-129.34	2.22	-17.51	-120.71	2.435	-16.88	-116.4
2.01	-18.76	-129.34	2.225	-17.51	-120.71	2.44	-16.88	-116.4
2.015	-18.76	-129.34	2.23	-17.51	-120.71	2.445	-16.88	-116.4
2.02	-18.76	-129.34	2.235	-17.51	-120.71	2.45	-16.26	-112.09
2.025	-18.76	-129.34	2.24	-17.51	-120.71	2.455	-16.26	-112.09
2.03	-18.76	-129.34	2.245	-17.51	-120.71	2.46	-16.26	-112.09
2.035	-18.76	-129.34	2.25	-17.51	-120.71	2.465	-16.26	-112.09
2.04	-18.76	-129.34	2.255	-17.51	-120.71	2.47	-16.26	-112.09
2.045	-18.76	-129.34	2.26	-17.51	-120.71	2.475	-16.26	-112.09
2.05	-18.76	-129.34	2.265	-17.51	-120.71	2.48	-16.26	-112.09
2.055	-18.76	-129.34	2.27	-17.51	-120.71	2.485	-16.26	-112.09
2.06	-18.76	-129.34	2.275	-17.51	-120.71	2.49	-16.26	-112.09
2.065	-18.76	-129.34	2.28	-17.51	-120.71	2.495	-16.26	-112.09
2.07	-18.76	-129.34	2.285	-17.51	-120.71	2.5	-16.26	-112.09
2.075	-18.13	-125.03	2.29	-17.51	-120.71	2.505	-16.26	-112.09
2.08	-18.13	-125.03	2.295	-17.51	-120.71	2.51	-16.26	-112.09
2.085	-18.13	-125.03	2.3	-16.88	-116.4	2.515	-16.26	-112.09
2.09	-18.13	-125.03	2.305	-16.88	-116.4	2.52	-16.26	-112.09
2.095	-18.13	-125.03	2.31	-16.88	-116.4	2.525	-16.26	-112.09
2.1	-18.13	-125.03	2.315	-16.88	-116.4	2.53	-16.26	-112.09
2.105	-18.13	-125.03	2.32	-16.88	-116.4	2.535	-16.26	-112.09
2.11	-18.13	-125.03	2.325	-16.88	-116.4	2.54	-15.63	-107.78
2.115	-18.13	-125.03	2.33	-16.88	-116.4	2.545	-15.63	-107.78
2.12	-18.13	-125.03	2.335	-16.88	-116.4	2.55	-15.63	-107.78
2.125	-18.13	-125.03	2.34	-16.88	-116.4	2.555	-15.63	-107.78
2.13	-18.13	-125.03	2.345	-16.88	-116.4	2.56	-15.63	-107.78
2.135	-18.13	-125.03	2.35	-16.88	-116.4	2.565	-15.63	-107.78
2.14	-18.13	-125.03	2.355	-16.88	-116.4	2.57	-15.63	-107.78
2.145	-18.13	-125.03	2.36	-16.88	-116.4	2.575	-15.63	-107.78
2.15	-18.13	-125.03	2.365	-16.88	-116.4	2.58	-15.63	-107.78
2.155	-18.13	-125.03	2.37	-16.88	-116.4	2.585	-15.63	-107.78
2.16	-18.13	-125.03	2.375	-16.88	-116.4	2.59	-15.63	-107.78
2.165	-18.13	-125.03	2.38	-16.88	-116.4	2.595	-15.63	-107.78
2.17	-18.13	-125.03	2.385	-16.88	-116.4	2.6	-15.63	-107.78
2.175	-18.13	-125.03	2.39	-16.88	-116.4	2.605	-15.63	-107.78
2.18	-18.13	-125.03	2.395	-16.88	-116.4	2.61	-15.63	-107.78
2.185	-18.13	-125.03	2.4	-16.88	-116.4	2.615	-15.63	-107.78

Time (s)	Press (mv)	Press (kPa)	Time (s)	Press (mv)	Press (kPa)	Time (s)	Press (mv)	Press (kPa)
2.16	-18.13	-125.03	2.375	-16.88	-116.4	2.59	-15.63	-107.78
2.165	-18.13	-125.03	2.38	-16.88	-116.4	2.595	-15.63	-107.78
2.17	-18.13	-125.03	2.385	-16.88	-116.4	2.6	-15.63	-107.78
2.175	-18.13	-125.03	2.39	-16.88	-116.4	2.605	-15.63	-107.78
2.18	-18.13	-125.03	2.395	-16.88	-116.4	2.61	-15.63	-107.78
2.185	-17.51	-120.71	2.4	-16.88	-116.4	2.615	-15.63	-107.78
2.19	-17.51	-120.71	2.405	-16.88	-116.4	2.62	-15.63	-107.78
2.195	-17.51	-120.71	2.41	-16.88	-116.4	2.625	-15.63	-107.78
2.63	-15.63	-107.78	2.845	-15.01	-103.47	3.06	-13.76	-94.85
2.635	-15.63	-107.78	2.85	-14.38	-99.16	3.065	-13.76	-94.85
2.64	-15.63	-107.78	2.855	-14.38	-99.16	3.07	-13.76	-94.85
2.645	-15.63	-107.78	2.86	-14.38	-99.16	3.075	-13.76	-94.85
2.65	-15.63	-107.78	2.865	-14.38	-99.16	3.08	-13.76	-94.85
2.655	-15.63	-107.78	2.87	-14.38	-99.16	3.085	-13.76	-94.85
2.66	-15.63	-107.78	2.875	-14.38	-99.16	3.09	-13.76	-94.85
2.665	-15.63	-107.78	2.88	-14.38	-99.16	3.095	-13.76	-94.85
2.67	-15.63	-107.78	2.885	-14.38	-99.16	3.1	-13.76	-94.85
2.675	-15.63	-107.78	2.89	-14.38	-99.16	3.105	-13.76	-94.85
2.68	-15.63	-107.78	2.895	-14.38	-99.16	3.11	-13.76	-94.85
2.685	-15.63	-107.78	2.9	-14.38	-99.16	3.115	-13.76	-94.85
2.69	-15.63	-107.78	2.905	-14.38	-99.16	3.12	-13.76	-94.85
2.695	-15.01	-103.47	2.91	-14.38	-99.16	3.125	-13.76	-94.85
2.7	-15.01	-103.47	2.915	-14.38	-99.16	3.13	-13.76	-94.85
2.705	-15.01	-103.47	2.92	-14.38	-99.16	3.135	-13.76	-94.85
2.71	-15.01	-103.47	2.925	-14.38	-99.16	3.14	-13.76	-94.85
2.715	-15.01	-103.47	2.93	-14.38	-99.16	3.145	-13.76	-94.85
2.72	-15.01	-103.47	2.935	-14.38	-99.16	3.15	-13.76	-94.85
2.725	-15.01	-103.47	2.94	-14.38	-99.16	3.155	-13.76	-94.85
2.73	-15.01	-103.47	2.945	-14.38	-99.16	3.16	-13.76	-94.85
2.735	-15.01	-103.47	2.95	-14.38	-99.16	3.165	-13.76	-94.85
2.74	-15.01	-103.47	2.955	-14.38	-99.16	3.17	-13.76	-94.85
2.745	-15.01	-103.47	2.96	-14.38	-99.16	3.175	-13.76	-94.85
2.75	-15.01	-103.47	2.965	-14.38	-99.16	3.18	-13.76	-94.85
2.755	-15.01	-103.47	2.97	-14.38	-99.16	3.185	-13.76	-94.85
2.76	-15.01	-103.47	2.975	-14.38	-99.16	3.19	-13.76	-94.85
2.765	-15.01	-103.47	2.98	-14.38	-99.16	3.195	-13.76	-94.85
2.77	-15.01	-103.47	2.985	-14.38	-99.16	3.2	-13.76	-94.85
2.775	-15.01	-103.47	2.99	-14.38	-99.16			
2.78	-15.01	-103.47	2.995	-14.38	-99.16			
2.785	-15.01	-103.47	3	-14.38	-99.16			
2.79	-15.01	-103.47	3.005	-13.76	-94.85			

4.4. TEST 1 GROUP

Test 1 group were conducted by using no coal dust while the methane concentrations varied. This group included six individual tests.

4.4.1. Pressure Profile

The monitored pressure inside the chamber was manually converted to the standard pressure unit (kPa). This is shown in Fig 4.3 - Fig 4.8. In this group, the peak pressure ranged from 5170 kPa to 6116 kPa. From the pressure curves, the piston was bounced 2 - 3 times in each test before it came to rest. Either from the pressure performance or from the physical observation, no fully confirmed ignitions occurred in this group. But, under the condition of a sufficiently high compression ratio methane can be ignited.

4.4.2. Temperature Profile

As stated previously, the temperature sensor responded slowly. It could not reflect the real variation of the temperature inside the chamber. So, it seemed to be of limited use in the laboratory tests. But, the temperature could be simulated by using the correspondent pressure profile under the condition of no chemical reaction.

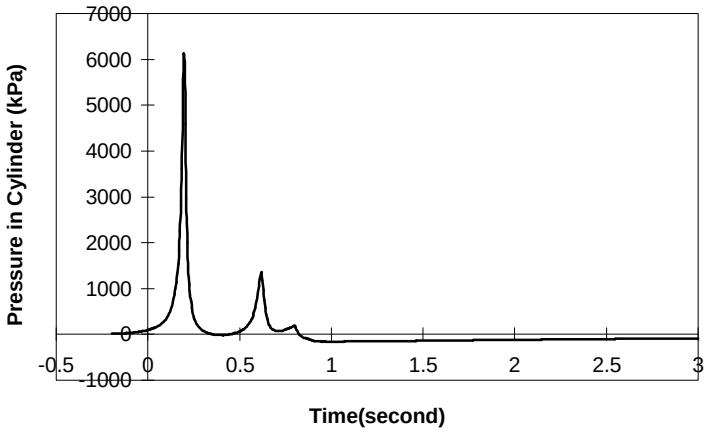

Fig 4.3. Variation in air pressure under coal dust 0 grams, methane concentration 0%, loads 600 kg, drop height 0.91 m and orifice diameter 1.6 mm.

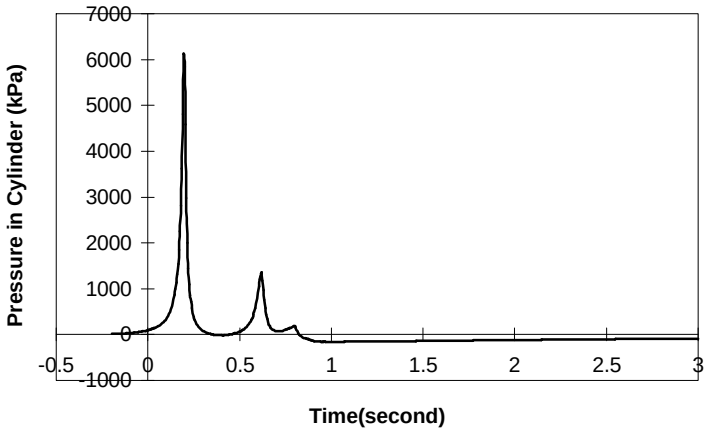

Fig 4.4. Variation in air pressure under coal dust 0 g/m^3, methane concentration 2.5%, loads 600 kg, drop height 0.91 m and orifice diameter 1.6 mm.

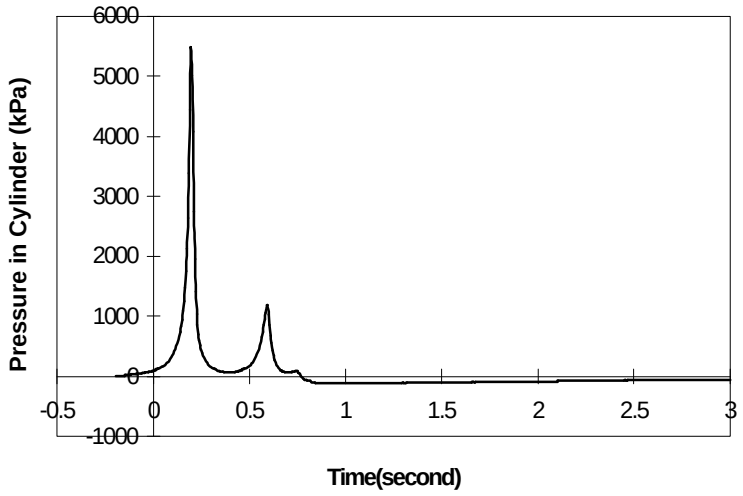

Fig 4.5. Variations in air pressure under coal dust 0 g/m^3, methane concentration 5%, loads 600 kg, drop height 0.91 m and orifice diameter 1.6 mm.

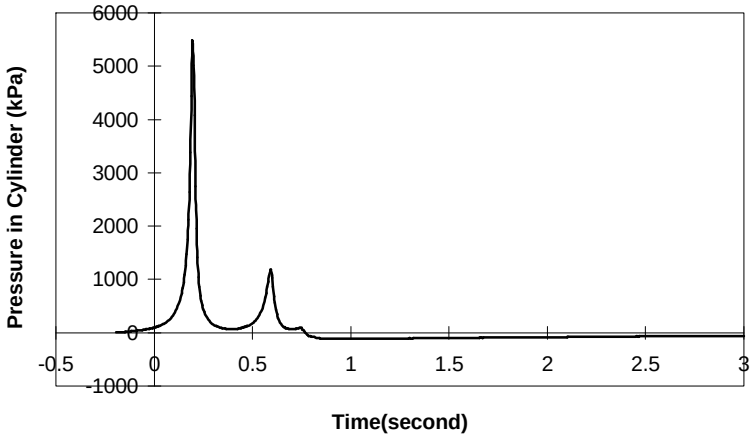

Fig 4.6. Variations in air pressure under coal dust 0 g/m^3, methane concentration 10%, loads 600 kg, drop height 0.91 m and orifice diameter 1.6 mm.

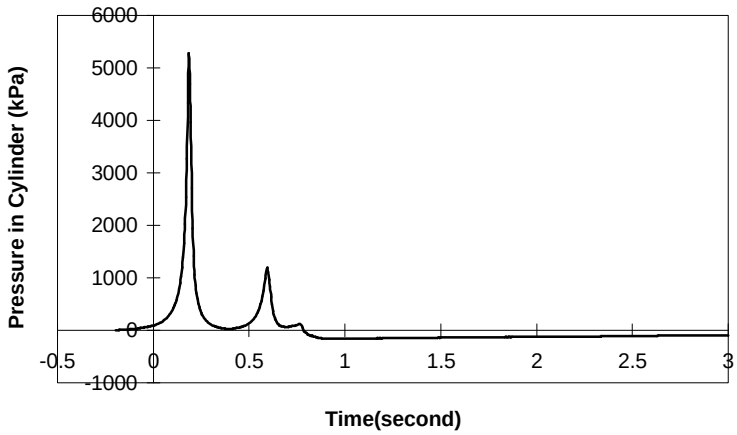

Fig 4.7. Variations in air pressure under coal dust 0 g/m^3, methane concentration 15%, loads 600 kg, drop height 0.91 m and orifice diameter 1.6 mm.

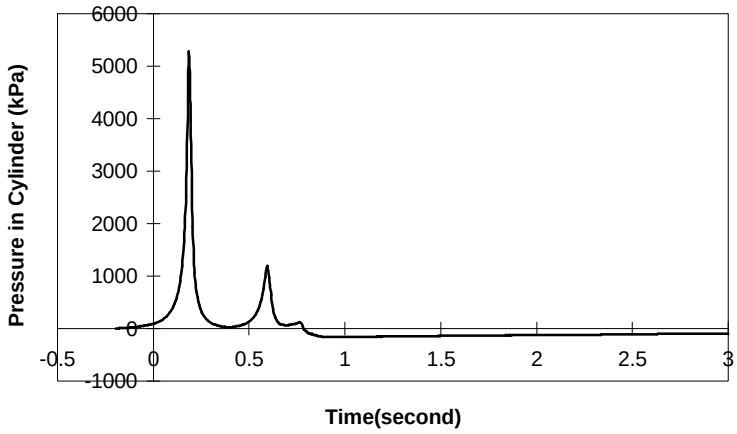

Fig 4.8. Variations in air pressure under coal dust 0 g/m^3, methane concentration 20%, loads 600 kg, drop height 0.91 m and orifice diameter 1.6 mm.

4.5. TEST 2 GROUP

Test 2 group were conducted by assuming constant coal dust (1316 g/m^3) while the methane concentrations varied. This group included six individual tests.

4.5.1. Pressure Profile

The recorded pressure signals (voltage) inside the chamber were manually transferred to the standard pressure unit (kPa). This is shown in Fig 4.9 - Fig 4.14. In this group, the peak pressure ranged from 4461 kPa to 17072 kPa. From the pressure profiles, the piston bounced at least 3 times in each test before it came to rest. When the methane concentrations were 5%, 10%, 15% by volume, respectively, obvious explosions occurred. This was confirmed not only by the astonishingly high peak pressure but also by the appearance of a jet of white flame from the outlet orifice. This also further verified that coal dust and methane are synergistic. In other tests of this group, no obvious ignitions happened although a test with coal dust alone produced smoke and the characteristic smell of burning coal.

4.5.2. Temperature Profile

Although the temperature sensor responsed slowly, it was still installed in the chamber. In the case of explosions, the temperature sensor was destroyed and needed to be replaced.

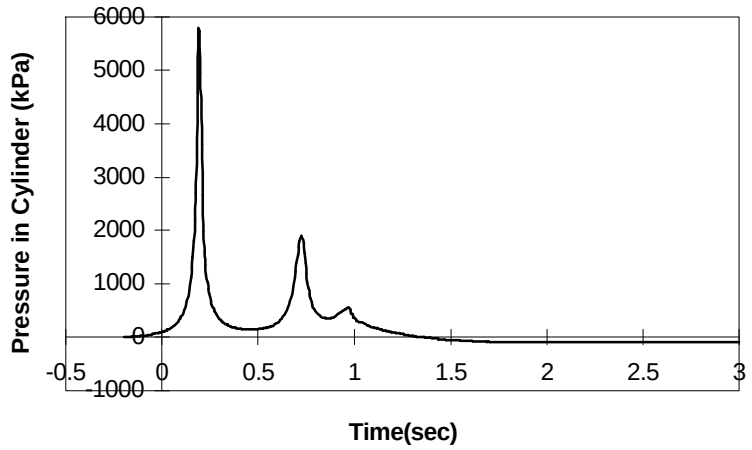

Fig 4.9. Variations in air pressure under coal dust 1316 g/m^3, methane concentration 0%, loads 600 kg, drop height 0.91 m and orifice diameter 1.6 mm.

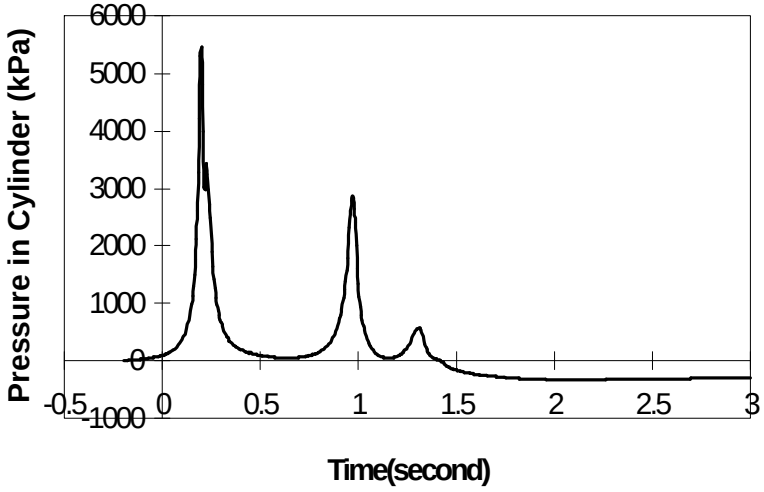

Fig 4.10. Variations in air pressure under coal dust 1316 g/m^3, methane concentration 2.5%, loads 600 kg, drop height 0.91 m and orifice diameter 1.6 mm.

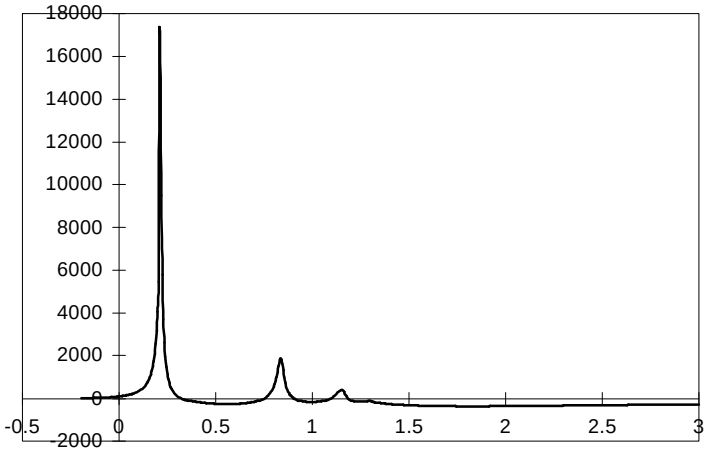

Fig 4.11. Variations in air pressure under coal dust 1316 g/m^3, methane concentration 5%, loads 600 kg, drop height 0.91 m and orifice diameter 1.6 mm.

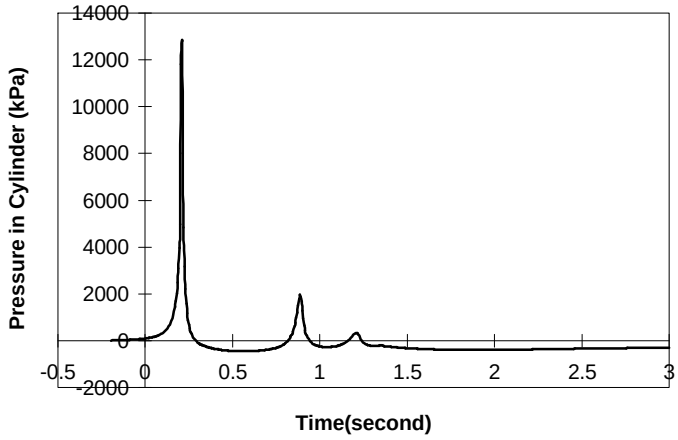

Fig 4.12. Variations in air pressure under coal dust 1316 g/m^3, methane concentration 10%, loads 600 kg, drop height 0.91 m and orifice diameter 1.6 mm.

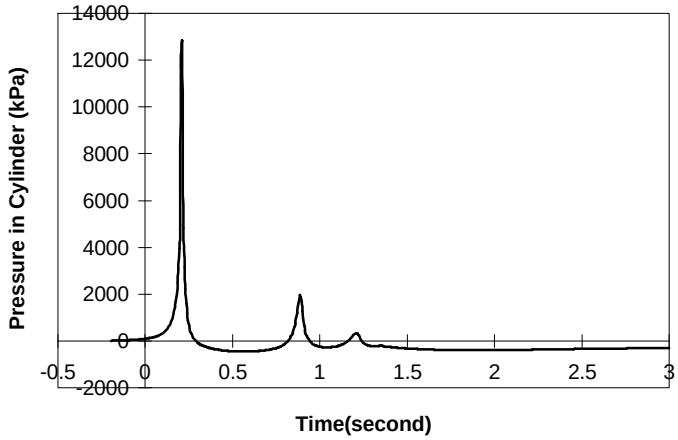

Fig 4.13. Variations in air pressure under coal dust 1316 g/m^3, methane concentration 15%, loads 600 kg, drop height 0.91 m and orifice diameter 1.6 mm.

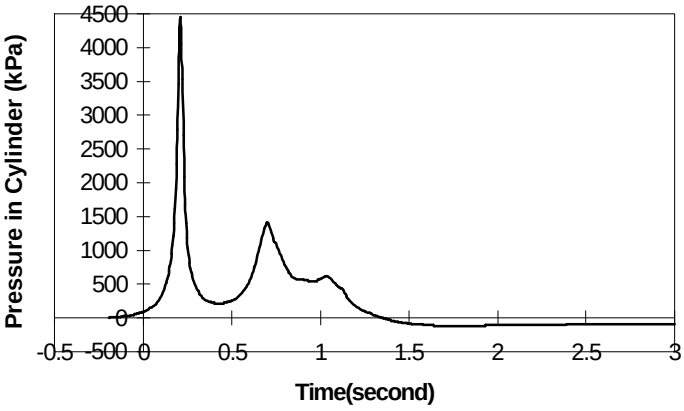

Fig 4.14. Variations in air pressure under coal dust 1316 g/m^3, methane concentration 20%, loads 600 kg, drop height 0.91 m and orifice diameter 1.6 mm.

Plate 4.4. A view of a typical explosion occurring in the group 2 tests.

4.6. TEST 3 GROUP

Test 3 group were conducted by assuming constant coal dust (2632 g/m^3) while the methane concentrations varied. This group included six individual tests.

4.6.1. Pressure Profile

The monitored pressure signals (voltage) inside the chamber were manually converted to the standard pressure unit (kPa). This is shown in Fig 4.15 - Fig 20. In this group, the peak pressure ranged from 4330 kPa to 13542 kPa. From the pressure curves, the piston bounced at least 2 times before it came to rest. When methane concentrations were 5%, 10%, 15% by volume, respectively, obvious explosions occurred. This was confirmed not only by the high peak pressure but also by the appearance of a jet of white flame from the outlet orifice. In other tests of this group, no obvious ignitions occurred although a test with coal dust alone did produce smoke and the characteristic smell of burning coal.

4.6.2. Temperature Profile

Although the temperature sensor responded slowly, it was still installed in the chamber in this group. In some cases of explosions, the destroyed temperature sensor needed to be replaced.

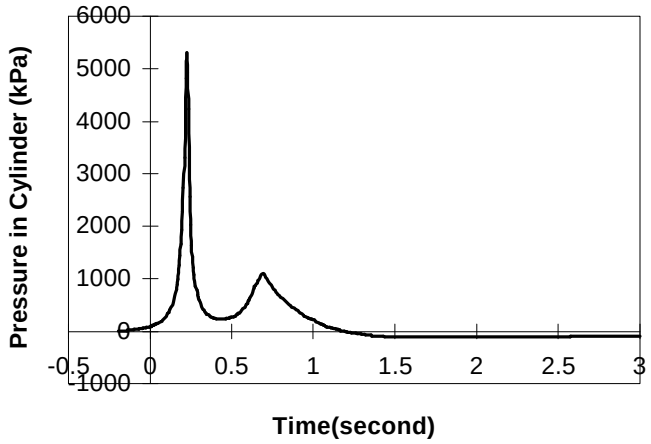

Fig 4.15. Variations in air pressure under coal dust 2632 g/m^3, methane concentration 0%, loads 600 kg, drop height 0.91 m and orifice diameter 1.6 mm.

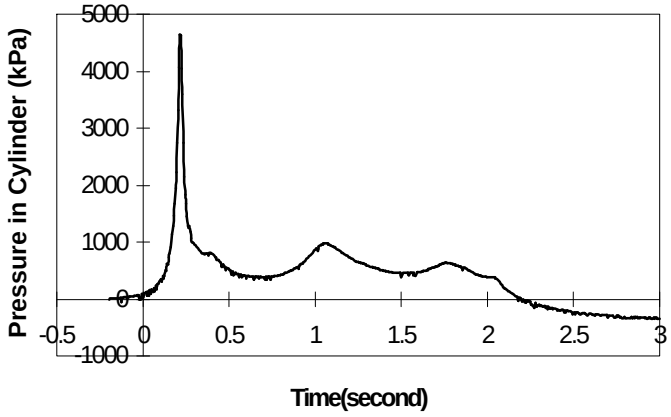

Fig 4.16. Variations in air pressure under coal dust 2632 g/m^3, methane concentration 2.5%, loads 600 kg, drop height 0.91 m and orifice diameter 1.6 mm.

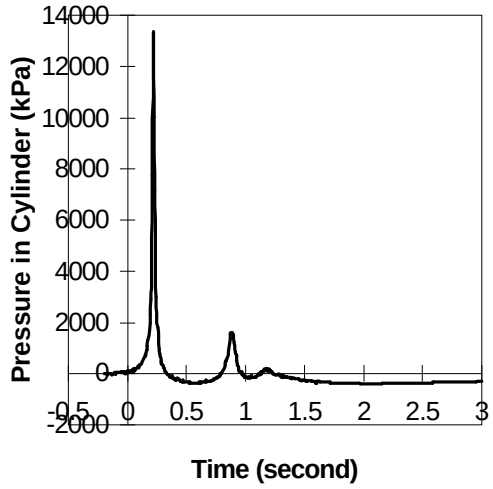

Fig 4.17. Variations in air pressure under coal dust 2632 g/m^3, methane concentration 5%, loads 600 kg, drop height 0.91 m and orifice diameter 1.6 mm.

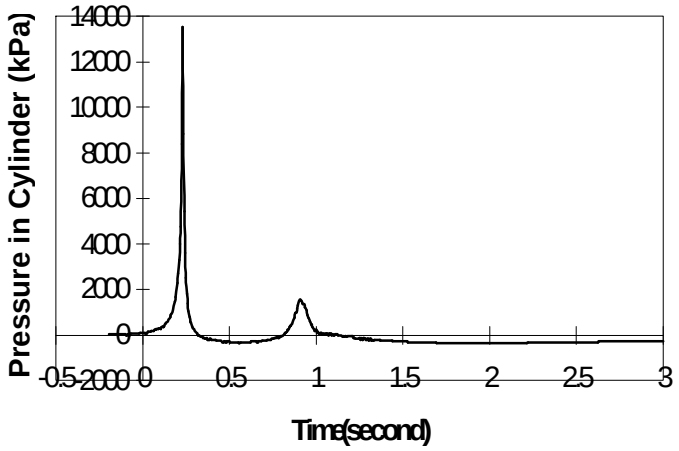

Fig 4.18. Variations in air pressure under coal dust 2632 g/m^3, methane concentration 10%, loads 600 kg, drop height 0.91 m and orifice diameter 1.6 mm.

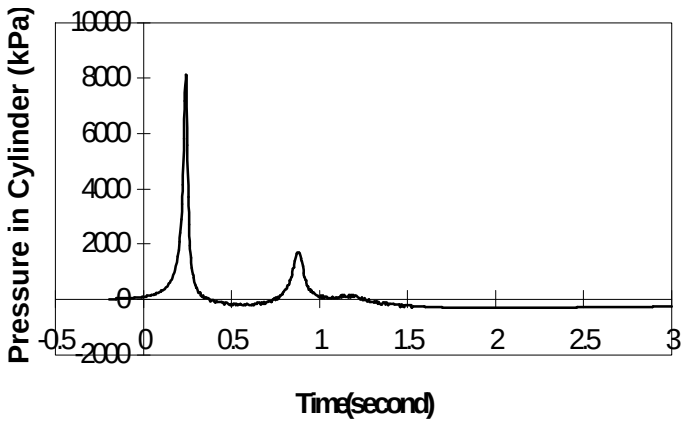

Fig 4.19. Variations in air pressure under coal dust 2632 g/m^3, methane concentration 15%, loads 600 kg, drop height 0.91 m and orifice diameter 1.6 mm.

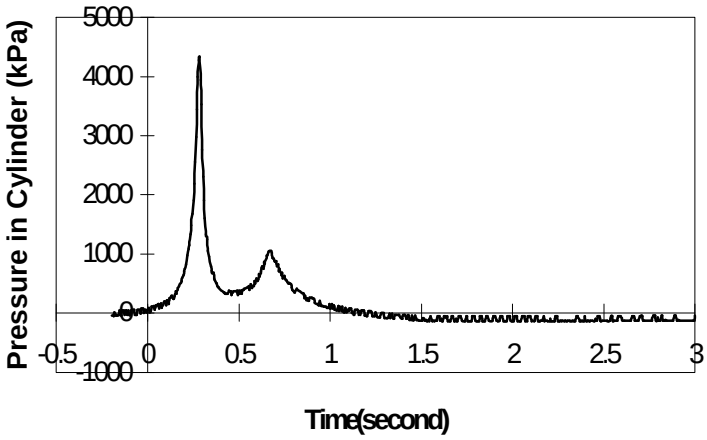

Fig 20. Variations in air pressure under coal dust 2632 g/m^3, methane concentration 20%, loads 600 kg, drop height 0.91 m and orifice diameter 1.6 mm.

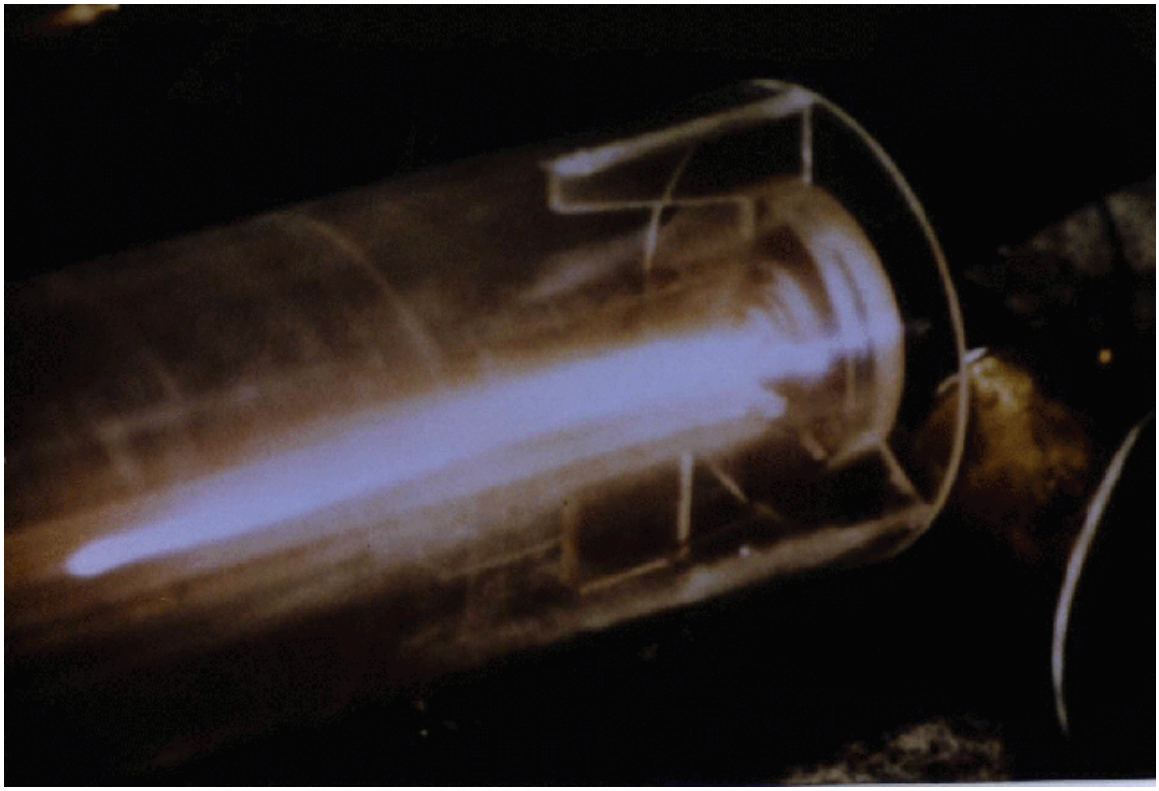

Plate 4.5. A view of a typical explosion occurring in the group 3 tests.

4.7. TEST 4 GROUP

Test 4 group were conducted by assuming constant coal dust (3948 g/m^3) while the methane concentrations varied. This group included six individual tests.

4.7.1. Pressure Profile

The recorded pressure signals (voltage) inside the chamber were manually converted to the standard pressure unit (kPa). This is shown in Fig 21 - Fig 26. In this group, the peak pressure ranged from 3613 kPa to 12108 kPa. From the pressure profiles, the piston bounced at least 2 times in each test before it came to rest. When the methane concentrations were 2.5%, 5%, 10% by volume, respectively, obvious explosions happened. This was confirmed not only by the astonishingly high peak pressure but also by the appearance of a jet of white flame from the outlet orifice. In this group, an explosion occurred at a methane concentration of 2.5% in the presence of a high concentration of coal dust. It is assumed that the upper flammability limits suggested by these results are imposed by the mixture becoming excessively fuel rich for an explosion to propagate.

4.7.2. Temperature Profile

Although temperature sensor responsed at 250 ms interval, it was still installed in the chamber in this group. Some destroyed temperature sensor needed to be replaced.

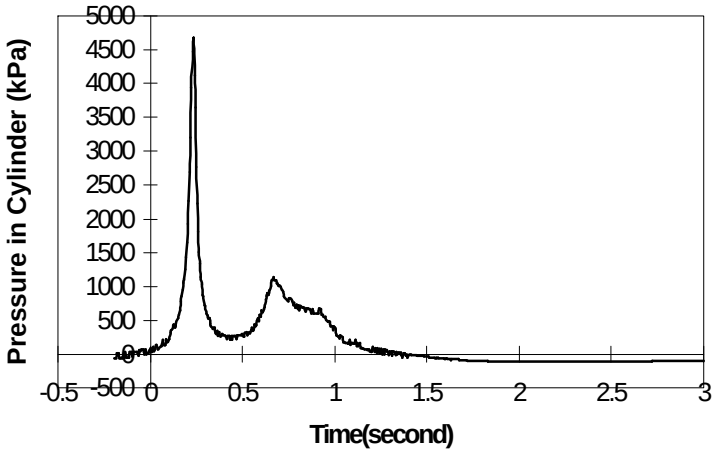

Fig 21. Variations in air pressure under coal dust 3948 g/m^3, methane concentration 0%, loads 600 kg, drop height 0.91 m and orifice diameter 1.6 mm.

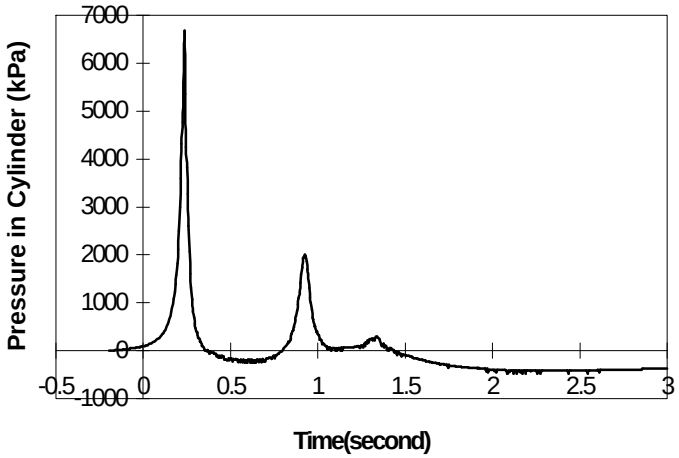

Fig 22. Variations in air pressure under coal dust 3948 g/m^3, methane concentration 2.5%, loads 600 kg, drop height 0.91 m and orifice diameter 1.6 mm.

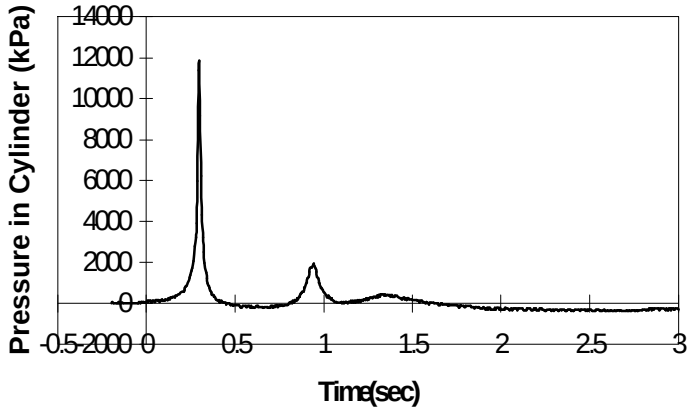

Fig 23. Variations in air pressure under coal dust 3948 g/m^3, methane concentration 5%, loads 600 kg, drop height 0.91 m and orifice diameter 1.6 mm.

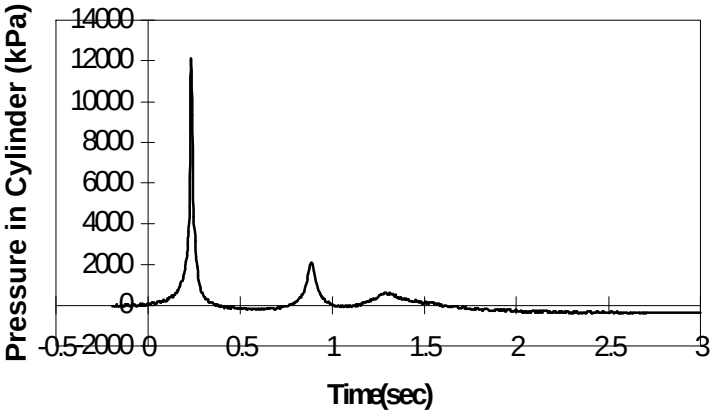

Fig 24. Variations in air pressure under coal dust 3948 g/m^3, methane concentration 10%, loads 600 kg, drop height 0.91 m and orifice diameter 1.6 mm.

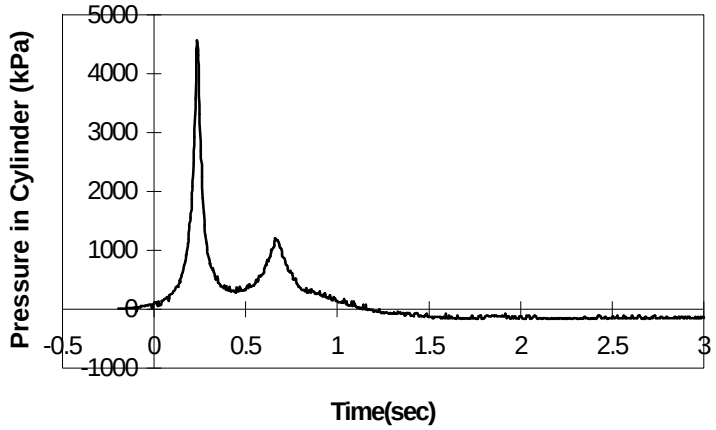

Fig 25. Variations in air pressure under coal dust 3948 g/m^3, methane concentration 15%, loads 600 kg, drop height 0.91 m and orifice diameter 1.6 mm.

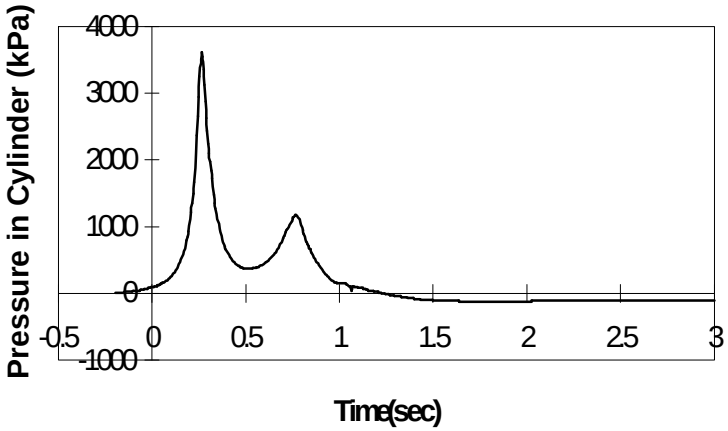

Fig 26. Variations in air pressure under coal dust 3948 g/m^3, methane concentration 20%, loads 600 kg, drop height 0.91 m and orifice diameter 1.6 mm.

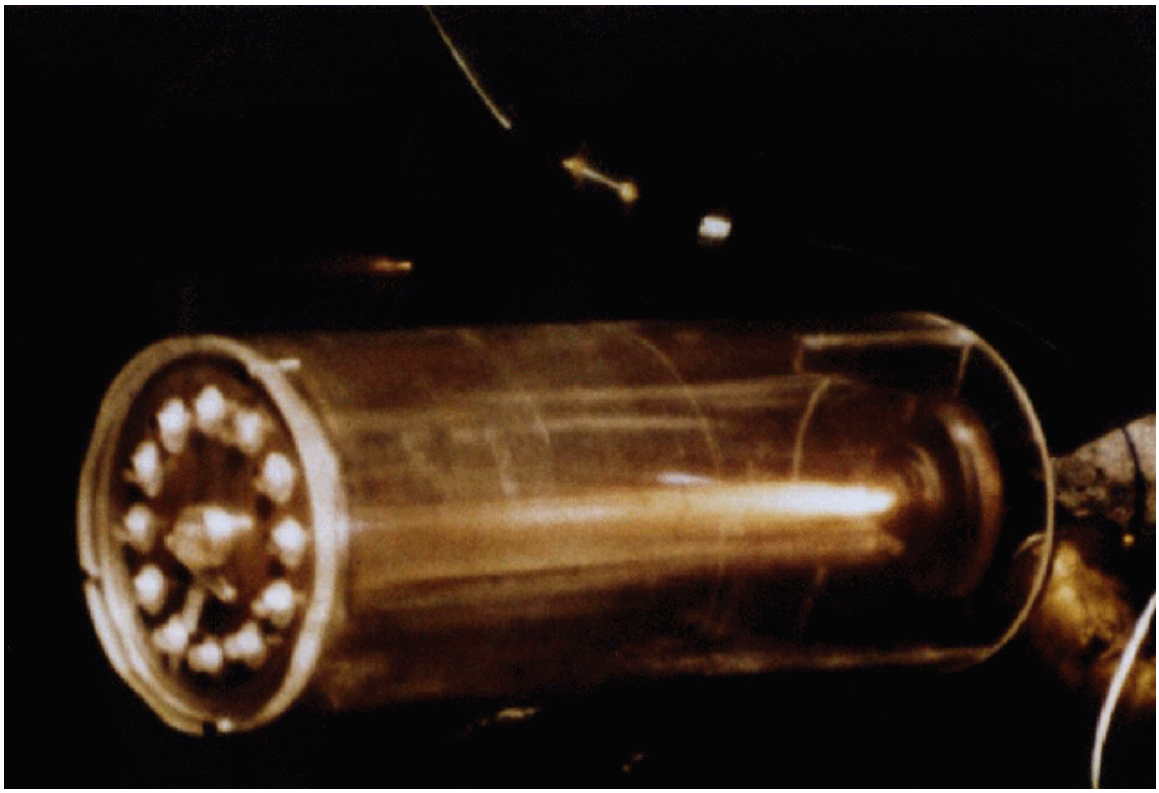

Plate 4.6. A view of a typical explosion occurring in the group 4 tests.

Chapter 5. Discussion, Conclusions and Recommendations

The purpose of this paper was to verify the possibility of ignition of air, methane and coal dust mixture when a large area of open gob collapses suddenly, by conducting a series of tests on a laboratory model. Theoretically, when a large roof is falling, the air under the roof beds is adiabatically compressed, i.e. negligible heat transfer to the surrounding rock surfaces. Controlled escape of air via interconnecting entries limits the build-up of air pressure. However, this same phenomenum causes the potential energy of the falling strata to be concentrated into a diminishing mass of air. This theoretical analysis resulted in the prediction that the temperature of the air would increase rapidly and continuously as the roof descends, reaching values that are capable of igniting methane and coal dust mixtures (Dr. McPherson, 1995a). As stated previously, although the laboratory model lacks the geometric similitude, the underlying principle is the same. If an explosion occurs under the laboratory condition, it also is possible under the real-life condition.

5.1. PRIMARY OBSERVATIONS

In this particular research, a total 24 of individual tests were completed. The initial trial tests during the development of the equipment had given experience of the pressures and temperatures obtained with differing loads and using air only. This led to a decision to maintain some test parameters unchanged for each test, such as the combined mass of the piston, supporting plate and concrete ballast at 600 kg (1320 lb) and outlet orifice diameter at 1.6 mm (0.0625 inches). The only test variables during the whole experiment were methane and coal dust concentrations. The methane concentrations were 0, 2.5, 5, 10, 15, 20% by volume. The coal dust concentrations employed were 0, 1316, 2632 and 3948 g/m^3. The lower flammability limit of coal dust may be of the order of 50 g/m^3 with maximum explosibility at 150 to 350 g/m^3 depending on the volatile content of the coal dust (Holding, 1982). The upper flammability limit might be as high as 5000 g/m^3 (Strang and McKenzie-Wood, 1985). Table 5.1 gives the variation of peak pressure (kPa) with different combinations of methane and coal dust for the whole experiment.

In the following Table, the shaded areas indicate that an explosion occurred. This was shown not only from abnormally high peak pressures but also from the appearance of a jet of white flame at the orifice outlet. During this particular series of laboratory tests, no ignition took place with methane alone, i.e. in the absence of coal dust. Although no anomalous high pressures nor flames were observed with coal dust alone in the air, several such tests produced smoke and the characteristic smell of burning coal. Obviously, when the compression ratio is sufficiently high, either coal dust or methane can be ignited. It is well known that a powered compression stroke in a diesel engine can be capable of igniting coal dust and, indeed, coal burning diesel engines have been built(ASME, 1992).

Table 5.1. Variation of peak pressure (kPa) with different combinations of methane and coal dust.

Methane **Coal Dust**	**0 %** **by volume**	**2.5**	**5**	**10**	**15**	**20**
0 (g/m^3)	**6116**	**5833**	**5461**	**5468**	**5288**	**5170**
1316	**5777**	**5466**	**17072**	**12804**	**12756**	**4461**
2632	**5310**	**4647**	**13280**	**13542**	**8115**	**4330**
3948	**4668**	**6688**	**11853**	**12108**	**4565**	**3613**

The effects of coal dust and methane are seen to be synergistic. Table 5.1 shows an explosion occurring at a methane concentration of 2.5% in the presence of a high concentration of coal dust. It is assumed that the upper flammability limits suggested by these results are imposed by an excessively fuel rich mixture for an explosion to propagate.

5.2. COMPUTER SIMULATION RESULTS

As stated previously, a computer program can be used to predict the variance of height, pressure and temperature. Fig 41 show the simulation results of height, air pressure and temperature for a laboratory test. The simulation parameters are: plan area = 0.0081 m^2, drop height = 0.92 m, load = 600 kg and no coal dust and methane. From Fig 5.1, the piston descends to near the bottom of the cylinder in about 0.5 second, then exhibits a single oscillation before settling into its equilibrium position. The effect of that oscillation is seen on the air pressure trace. That reaches an initial peak of some 6000 kPa (absolute) with a corresponding air temperature of approximately 1300 ^{o}C. The second peak of pressure is interrupted by the piston reaching its final position, after which continued dissipation of the air from the cylinder results in the air pressure falling to normal atmospheric conditions. However, the air temperature continues to ascend during the final stages of the drop. This is because the gravitational work is expended against a decreasing mass of air under the piston. The specific internal energy of that decreasing mass soars and, with it, the temperature. The temperature reaches a temperature capable of igniting coal dust. Because of heat transfer with the surrounding materials, the temperature becomes indeterminate after movement of the piston has ceased.

Fig 5.2 gives the comparison between the simulated pressure curve and the actual pressure trace recorded during a drop test on air with no coal dust or methane. It is found that the practical and simulated pressure curves are very similar. The simulation results are reasonable.

5.3. CONCLUSION

The laboratory results reported in this thesis prove conclusively that compression of a mixture of air, coal dust and methane by a falling weight can result in an ignition. Furthermore, the results confirm previous observations that the flammable components are synergistic, the presence of one assisting the ignition of the other. The computer model developed to simulate the adiabatic compression of air under a falling weight has been improved to take account of voidage left in the gob after a collapse and to produce a better representation of the flowpaths leading away from the collapse zone. The agreement obtained between the model and the laboratory results holds promise that the former can be employed to indicate the level of potential hazard in any given mine.

This work has further verified the possibility of adiabatic ignitions in collapsing mine workings. The effect will also enhance the probability of ignitions by frictional effects involving sandstone or pyritic rock. Nevertheless, the conditions under which adiabatic ignitions can occur are sufficiently stringent for the phenomenum to be regarded as uncommon. First, the plan area of the fall must be large so that the reducing space under the falling material offers a significant resistance to the displacement of the air. The numerical simulation for full-scale application becomes unstable at areas of less than 20 x 20 m. Secondly, the roof material must descend near simultaneously over the collapsing zone rather than the rolling motion that often takes place in failing gob area. Furthermore, there must exist, or the fall must generate, a mixture of air, coal dust and methane that is capable of being ignited.

5.4. RECOMMENDATIONS

The theoretical predictions and laboratory results indicate that it is possible to ignite a mixture of air, methane and coal dust when a large roof fall occurs in an underground coal mine. In order to obtain better understanding about the mechanism of the explosion, if necessary, some further work needs to be concentrated on the following areas:

- The numerical analysis assumed that the escape of air from the collapse zone has been based on stead - flow relations. The further work should take account into the inertial effects of accelerating the air and the formation of shock waves within that escaping air.

- The chemical reaction process is very complicated during an explosion. The mechanism of the reaction and the prediction of the temperature behavior should further be studied.

- The minimum plan area of a roof for a given coal dust and methane concentrations in

which an explosion could occur should be established.

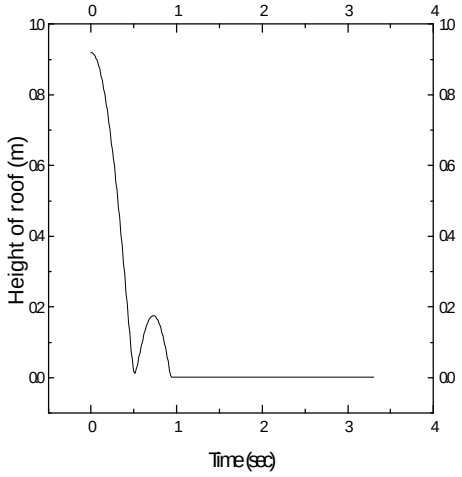

(a)

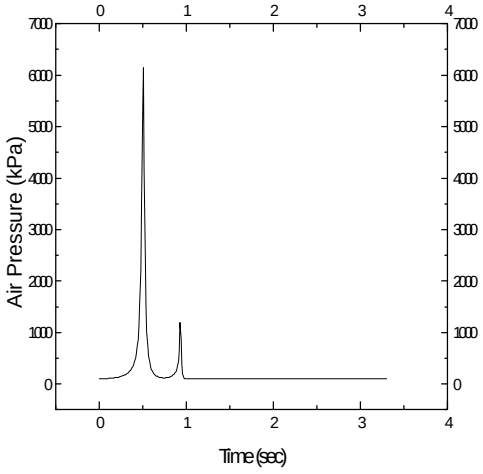

(b)

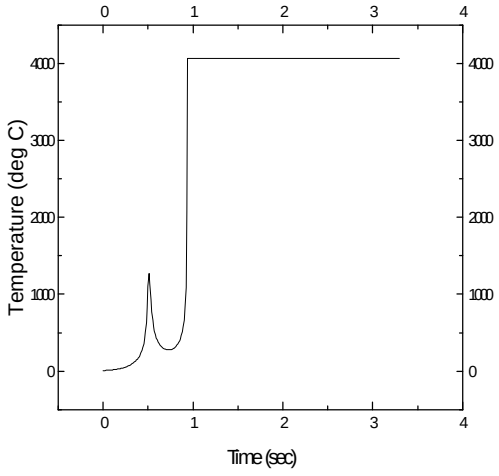

(c)

Fig 5.1. The simulation results of height(a), air pressure(b) and temperature(c) for a laboratory test.

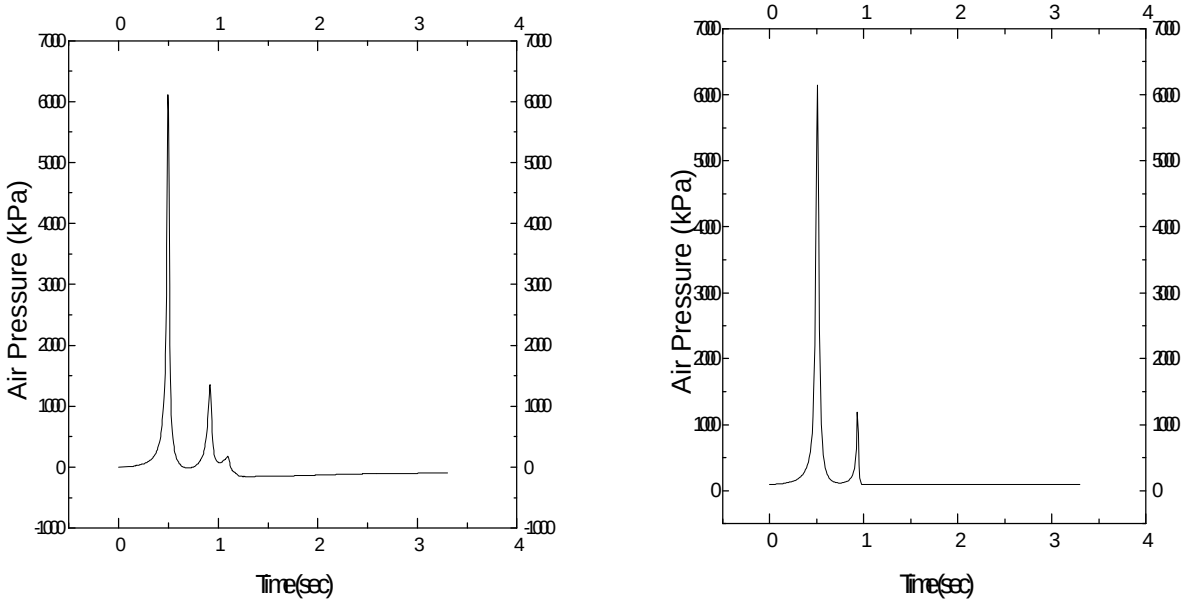

(a) (b)

Fig 5.2. Comparison between the actual pressure trace(a) and the simulated pressure curve(b) during a laboratory test without methane and coal dust.

Appendix: A computer simulation program (Written by Dr. McPherson in BASIC)

```
5 OPEN “HTAB.DAT” FOR OUTPUT AS #1
10 OPEN “PTAB.DAT” FOR OUTPUT AS #2
15 OPEN “TTAB.DAT” FOR OUTPUT AS #3
16 OPEN “PCTAB.DAT” FOR OUTPUT AS#4
17 DEFDBL M-Z
18 PO = 100000
20 TE = 283.15
25 RT = 0 * 10 ^ 10: A = 0.0081: MR = 600
26 R = 287.04: RTS = 0.2 * 10 ^ 10: RTO = 1 * 10 ^ 10
27 PC = 100000: VC = 0.00012
30 RTT = RT
35 T1 = TE
40 P1 = PO: P = PO: DT = 0.0001
41 PI = PO
45 U = 0: I = 0: T = 0: Z = 0.92: K = 1.4: DF = 1.1
50 C = PO * Z ^ 1.4
55 V = A * Z: MA = P * V / (287.04 * TE): RA = MA / V
57 J = ABS(I / 100 - INT(I / 100))
60 IF J > 0.001 THEN GOTO 78
65 PRINT #1, USING “###.###” ; T; :PRINT #1, USING “#####.###” ;Z
70 PRINT #2, USING “###.###” ; T; :PRINT #2, USING “#########” ; P / 1000
75 PRINT #3, USING “###.###” ; T; :PRINT #3, USING “######.##” ; (TE - 273.15)
76 PRINT #4, USING “###.###” ; T; :PRINT #4, USING “#########” ; PC / 1000
78 IF U > = 0 THEN GOTO 82
80 DU = (9.810001 - (P - PO) * A / MR + DF * U) * DT
81 GOTO 95
82 DU = (9.810001 - (P - PO) * A / MR - DF * U) * DT
95 U = U + DU
100 Z = Z - U * DT
101 IF Z > 0.001 THEN GOTO 105
102 Z = 0.001: GOTO 110
105 P = C / Z ^ K
110 TE = T1 * (P / P1) ^ ((K - 1) / K)
115 T1 = TE
120 RA = P / (287.04 * TE)
125 DMA = SQR(ABS((P - PC) * RA / RTS)) * DT
126 IF PC > P THEN DMA = - DMA
130 MA = MA - DMA
135 DP = 287.04 * TE * DMA / (A * Z)
```

```
140 P = P - DP
141 DPC = DMA * R * TE / VC
142 PC = PC + DPC
143 RAC = PC / (R * TE)
144 DMO = SQR(ABS((PC - PO) * RAC / RTO)) * DT
145 IF PO > PC THEN DMO = - DMO
146 DPC = DMO * R * TE / VC
147 PC = PC - DPC
149 I = I + 1: T = T + DT
150 P1 = P
155 C = P * Z ^ K
165 IF I < 33000 THEN GOTO 57
200 PRINT #1, USING “###.###” ; T; :PRINT #1, USING “#####.###” ;Z
205 PRINT #2, USING “###.###” ; T; :PRINT #2, USING “#########” ; P / 1000
210 PRINT #3, USING “###.###” ; T; :PRINT #3, USING “######.##” ; (TE - 273.15)
215 PRINT #4, USING “###.###” ; T; :PRINT #4, USING “#########” ; PC / 1000
220 END
```

References

Anonymous, Omega Instrumentation and Reference Yearbook, vol27. Supplement, Omega Engineering, Inc., Stanford, CT, 1991, pp. B-246.

Anonymous, Low Impedance Quartz Pressure Transducers, Series 100, PCB Piezotronics, Inc., Depew, NY, Publication S 100993, 1993, pp. 26-27.

Anonymous, Notification, Investigation, Reports and Records of Accidents, Injuries, Employment, and Coal Production in mines, Code of Federal Regulations, Mineral Resources, CFR Title 30, Part 50, Washington D. C.

Anonymous, Allis-Chalmers Operators Manual, Data Precision, Inc., 1985.

ASME Conferences, Coal-Fueled Diesel Engines: American Society of Mechanical Engineers, Annual Energy Sources Technology Conferences, Texas, 1989.

ASME Conferences, Coal-Fueled Diesel Engines: American Society of Mechanical Engineers, Annual Energy Sources Technology Conferences, Texas, 1992.

Bin, H., Use of Fracture Mechanics Parameters to Characterize Comminution, MS Thesis, Virginia Polytechnic Institute and State University, 1996.

Bryan, et al., Some Problems of Strata Control and Support in Pillar Workings, The Mining Engineer, No. 41, Feb, 1964, pp. 238-254.

Dixon, D. W., Ediz, I. G., and Fidler, W. M., A New Method for the Arresting of Underground Tunnel Explosions, SME, 7th U.S. Symposium on Mine Ventilation, Lexington, Kentucky, 1995, pp.245-250.

Donald, W. M., Mine Fires: Prevention, Detection, Fighting, Maclean Hunter Publishing Company, 1990, pp. 1-15.

Ediz, I. G., Gorgulu, A., and Dixon, D.W., A New Approach for Arresting the Propagation of Coal Dust Explosions-AGE. 1 Active Flame Proof Door, Proceedings of the 13th Mining Congress of Turkey, Istanbul, 1993, pp.79-90.

Elio, L. C., and David, R. Z., Lightning Strikes and Mine Explosions, SME, 7th U.S. Symposium on Mine Ventilation, Lexington, Kentucky, 1995, pp.245-250.

Holden, W., Explosible Dusts. Environmental Engineering in South African Mines, Published by the Mine Ventilation Society of South Africa, 1982, pp. 763-771.

Lewis, B., Combustion, Flames and Explosions of Gases, Academic Press Inc., 1961, pp. 199-381.

Lidin, G. D., et al., Control of Methane in Coal Mines, English Translation Catalog No. 1190, Israel Program for Scientific Translations, Original in Russian 1961, 1964, pp. 1-9.

Loomis, I. M., Application of Water Mist to Fuel-Rich Fires in Model Coal Mine Entries, MS Thesis, Virginia Polytechnic Institute and State University, 1995.

McPherson, M. J., 1995a, The Adiabatic Compression of Air by Large Falls of Roof, SME, 7th U.S. Symposium on Mine Ventilation, Lexington, Kentucky, 1995, pp.257-262.

McPherson, M. J., X, Wu. and Karfakis, M. G., 1995b, The Compression of Air under Large Falls of Roof, 26th International Conference of Safety in Mines Institutes, Katowice, Poland, 1995.

McPherson, M. J., Air Pressure Developed in Collapsing Workings, Trans. 2nd International Mine Ventilation Congress, Reno, Nevada, Society of Mining Engineering, 1980, pp. 317-325.

McPherson, M. J., Subsurface Ventilation and Environmental Engineering, Chapman and Hall, 1993.

Powell, F and Billinge, K., The Frictional Ignition Hazard Associated With Colliery Rocks, The Mining Engineer, No. 174, July, 1975, pp. 527-531.

Steven, J. S. A Characterization of Frictional Ignitions in Underground Coal Mines, SME, 7th U.S. Symposium on Mine Ventilation, Lexington, Kentucky, 1995, pp.263-268

Song, Y. and Xu, L., Study of the Impact of Mining Under Massive Roof at Datong Coal Mines, China, Proceedings, 11th International Conference on Ground Control in Mining, Wollongong, Australia, 1992, pp. 540-547.

Timko, R. J., and F. N. Kissel, Hazards of Underground Coal Mine Fires, Society for Mining , Metallurgy, and Exploration, Inc. Preprint Number 93-121, Reno, Nevada, Feb, 1993, pp. 7.

Trevits, M. A., Finfinger, G. L., and LaScola, L. C., Evaluation of U.S. Coal Mine Emissions, Preprint Number 93-154, Society of Mining Engineers Annual Meeting, Reno, Nevada, Feb, 1993, pp. 7.

Van Wylen, G. J., and R. E. Sonntag, Fundamentals of Classical Thermodynamics, 3rd Edition English/SI Version, John Wiley and Sons, New York, 1986.

Vos, A. D., Coal Dust Explosions, Their Prevention and Control, Journal of the Mine Ventilation Society of South Africa, vol. 27, No. 6, June, 1974.

Waclaw, C., Coal Dust Explosions and Their Suppression, Translated from Polish by the Foreign Scientific Publications Department of the National Center for Scientific, Technical and Economic Information, 1975, pp. 1-40.

Wei, L and McPherson, M. J., The Ignition of Methane and Coal Dust by Compression in Collapsing Gob Areas, India, 1996,

Vita

Wei Lin

Wei Lin was born in Wanxian City, Sichuan Province, P. R. China. He graduated from the Kunming University of Science and Technology (Formerly Kunming Institute of Technology) with a B.S. in mining engineering in 1984. He then worked at Safety and Environmental Protection Research Institute, Ministry of Metallurgical Industry of China, for more than ten years as a mining engineer. He came to Virginia Polytechnic Institute and State University in 1995.